Insights into glacial processes from micromorphology of silt-sized sediment

Allison P. Lepp[1], Lauren E. Miller[1], John B. Anderson[2], Matt O'Regan[3], Monica C.M. Winsborrow[4], James A. Smith[5], Claus-Dieter Hillenbrand[5], Julia S. Wellner[6], Lindsay O. Prothro[7], Evgeny A. Podolskiy[8]

[1]Department of Environmental Sciences, University of Virginia, Charlottesville, VA 22903, USA
[2]Department of Earth Science, Rice University, Houston, TX 77005, USA
[3]Department of Geological Sciences, Stockholm University, 10691 Stockholm, Sweden
[4]iC3: Centre for ice, Cryosphere, Carbon and Climate, Department of Geosciences, UiT the Arctic University of Norway, 9037 Tromsø, Norway
[5]British Antarctic Survey, Natural Environment Research Council, High Cross, Madingley Road, Cambridge, CB3 0ET, UK
[6]Department of Earth and Atmospheric Sciences, University of Houston, Houston, TX 77204, USA
[7]Department of Physical and Environmental Sciences, Texas A&M University - Corpus Christi, Corpus Christi, TX 78412, USA
[8]Arctic Research Center, Hokkaido University, Sapporo, Hokkaido 001-0021, Japan

Correspondence to: Allison P. Lepp (apl2jt@virginia.edu)

Abstract. Silt-rich meltwater plume deposits (MPDs) analyzed from marine sediment cores have elucidated clearly connected, yet difficult to constrain, relationships between subglacial hydrology, ice-marginal landforms, and grounding-zone retreat patterns for several glacial catchments. Few attempts have been made to infer details of subglacial hydrology, such as flow regime, geometry of drainage pathways, and mode(s) of sediment transport through time from grain-scale characteristics of MPDs. Using sediment samples from MPD, till, and grounding-zone proximal diamicton collected offshore of six modern and relict glacial catchments in both hemispheres, we examine grain-shape distributions and microtextures (collectively, grain micromorphology) of the silt fraction to explore whether grains are measurably altered from their subglacial sources via meltwater action. We find that 75 % of all imaged grains (n = 9,400) can be described by 25 % of the full range of measured shape morphometrics, indicating grain-shape homogenization through widespread and efficient abrasive processes in subglacial environments. Although silt grains from MPDs exhibit edge rounding more often than silt grains from tills, grain surface textures indicative of fluvial transport (e.g., v-shaped percussions) occur in only a modest number of grains. Furthermore, MPD grain surfaces retain several textures consistent with transport beneath glacial ice (e.g., straight or arcuate steps, (sub)linear fractures) in comparable abundances to till grains. Significant grain-shape alteration in MPDs compared to their till sources is observed in sediments from glacial regions where (1) high-magnitude, potentially catastrophic, meltwater drainage events are inferred from marine sediment records, and (2) submarine landforms suggest

1

supraglacial melt contributed to the subglacial hydrological budget. This implies that quantifiable grain-shape alteration in MPDs could reflect a combination of high-energy flow of subglacial meltwater, persistent sediment entrainment, and/or long sediment transport distances through subglacial drainage pathways. Integrating grain micromorphology into analysis of MPDs in site-specific studies could therefore aid in distinguishing periods of persistent, well-connected subglacial discharge from periods of sluggish or disorganized drainage. In the wider context of deglacial marine sedimentary and bathymetric records, a grain micromorphological approach may bolster our ability to characterize ice response to subglacial meltwater transmission through time. This work additionally demonstrates that glacial and fluvial surface textures are retained on silt-sized quartz grains in adequate amounts for microtexture analysis which has heretofore been conducted exclusively on the sand fraction. Therefore, grain microtextures can be examined on silt-rich glaciogenic deposits that contain little to no sand as a means to evaluate sediment transport processes.

1 Introduction

The distribution and transmission of water beneath ice sheets influences pressure at the ice-bed interface (Bindschadler, 1983), subglacial sediment deformation (Alley et al., 1986; Boulton et al., 2001; Iverson, 2010) and, subsequently, ice-flow dynamics (e.g., Stearns et al., 2008; Gustafson et al., 2022; Livingstone et al., 2022 and references therein). Because quantities of ice sheet surface melt production and drainage to ice-sheet beds are modeled to increase in coming decades (Trusel et al., 2015; Lenaerts et al., 2016; Flowers, 2018; Gilbert and Kittel, 2021), continued efforts towards a nuanced understanding of subglacial hydrology at all scales is needed. Evidence of sediment-laden subglacial meltwater discharge into the ocean is preserved in the marine sediment record, and sediment cores from deglaciated continental shelves are therefore valuable archives of paleo-subglacial drainage. Distinctive meltwater plume deposits (MPDs) recovered offshore extant ice sheets have been used to identify discrete meltwater drainage events and evaluate persistence of subglacial drainage pathways, with temporal resolutions of centuries to millennia (Witus et al., 2014; Prothro et al., 2018; O'Regan et al., 2021; Jennings et al., 2022; Lepp et al., 2022). When integrated into glaciomarine facies models, these relatively well-sorted, silt-rich MPDs reveal connections between subglacial hydrologic activity and ice-marginal behavior prior to and during glacial retreat (Simkins et al., 2017; Prothro et al., 2018; O'Regan et al., 2021). However, targeted studies that attempt to infer details of paleo-subglacial hydrology, such as the evolution of drainage pathways or sediment mobilization within subglacial meltwater flow, from MPDs are lacking.

Research characterizing MPDs has largely relied on grain size (Witus et al., 2014; Simkins et al., 2017; Prothro et al., 2018, 2020), magnetic susceptibility (Witus et al., 2014; Smith et al., 2017), sediment structure (O'Regan et al., 2021; Lepp et al., 2022; Lešić et al., 2022; Jennings et al., 2022; Clark et al., 2024), and water content (Streuff et al., 2017; Lepp et al., 2022; Clark et al., 2024) to distinguish these deposits from other glaciomarine sediments. In acoustic data, sediments that compose MPDs appear stratified and drape the seafloor topography (Witus et al., 2014; Hogan et al., 2020a; Jennings et al., 2022; Lepp et al., 2022; Roseby et al., 2022) reflective of suspension settling, and may infill bathymetric depressions (e.g.,

Nitsche et al., 2013; Witus et al., 2014; Roseby et al., 2022). In sediment cores, MPDs are often laminated or thinly bedded, where subtle variations in grain size between laminae may indicate varying plume dynamics, magnitude of drainage events, or proximity of the grounding zone (Ó Cofaigh and Dowdeswell, 2001; O'Regan et al., 2021; Jennings et al., 2022; Lepp et

70 al., 2022; Roseby et al., 2022). Shared grain size modes (Simkins et al., 2017; Prothro et al., 2018) and geochemical similarities (Lepp et al., 2022) between subglacial tills, grounding-zone proximal deposits, and MPDs from the same region substantiate the hypothesis that these deposits share a common subglacial origin. Furthermore, the grain-size distributions of MPDs collected offshore from several Antarctic ice-sheet drainage sectors are strikingly similar despite regional variations in subglacial geology (Halberstadt et al., 2016; Simkins et al., 2017; Prothro et al., 2018; Lepp et al., 2022). This similarity

75 suggests the glacial and/or glaciofluvial processes that produce these sedimentary deposits operate on an ice-sheet-wide scale, but such processes are poorly understood. Furthermore, hypothesized mechanisms for subglacial mobilization and sorting of MPDs observed offshore (e.g., Schroeder et al., 2019) have not been empirically evaluated.

Grain shape is a function of bedrock geology, weathering effects, and sediment transport mechanisms (Mahaney, 2002). It is therefore a powerful proxy for inferring sediment transport history and depositional setting (e.g., Oakey et al.,

80 2005; Campaña et al., 2016; van Hateren et al., 2020), but has been underused in studies that characterize glacial deposits. Of those sparse works, many employ Fourier grain-shape analysis to identify harmonic ranges describing grain elongation and roughness which are then used to infer sediment transport history (Wellner et al., 2011; Livsey et al., 2013; Witus et al., 2014; Charpentier et al., 2017; Robinson et al., 2021; Clark et al., 2024). In Pine Island Bay, West Antarctica, a comparison of till grains to MPD grains showed differences in elongation but little variation in grain roughness (Witus et al., 2014),

85 providing support for the use of grain shape in glaciomarine environments as an indicator of subglacial sediment transport. Complementary to grain shape, grain microtextures have been more widely examined on the surfaces of glaciogenic sand-sized grains (cf. Mahaney, 2002; Vos et al., 2014). Various suites of microtexture assemblages are associated with different genetic processes; the high pressures, abrasion, and grinding that occur through subglacial sediment transport manifests in surface textures such as straight or arch-shaped steps, abrasion of grain edges, and series of (sub)linear fractures (Mahaney,

90 2002). This contrasts with surface textures like v-shaped percussions or impact pits that form through inter-granular collisions, and which are commonly observed on grains from fluvial environments (Mahaney, 2002). Microtextural analysis has been employed to distinguish sources of ice-rafted debris (Immonen, 2013; St. John et al., 2015; Passchier et al., 2021), infer relative ice volume on glacial-interglacial timescales (Cowan et al., 2008), and evaluate distance of proglacial sediment transport (Sweet and Brannan, 2016; Křížek et al., 2017).

95 This study combines quantitative grain shape measurements with qualitative microtexture analysis to characterize and compare MPDs to subglacial tills (or to grounding-zone proximal deposits, if till is unavailable) from six currently glaciated and formerly glaciated settings in both hemispheres. The sediments examined were collected offshore from the contemporary Ryder Glacier in northwestern Greenland, Pine Island and Thwaites glaciers in West Antarctica, and in the western Ross Sea, West Antarctica, and from the deglaciated seafloor in Marguerite Trough on the western Antarctic

100 Peninsula shelf, and from Thor Iversenbanken in the central Barents Sea (Fig. 1). We aim to determine whether MPDs have
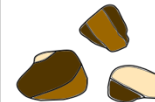
distinctive grain-shape distributions and microtexture assemblages and to explore how grain-shape alteration in MPDs, when compared to grains in their source sediments, may record process-based details of subglacial grain-size production, sediment transport, and evolution of subglacial plumbing. Our ability to more clearly relate changes in glaciomarine sediment records to changes in subglacial hydrological conditions through time is critical to advance our understanding of glacial sensitivity and response to subglacial water transmission and organization.

1.1 Bathymetric and glaciological settings of study sites

Ryder Glacier drains from the northwestern Greenland Ice Sheet into the Lincoln Sea through the Sherard Osborn Fjord (Fig. 1; O'Regan et al., 2021). Cores sampled for this study were recovered from an along-fjord transect at sites ranging in water depths from 238 m to 633 m (Table A1). Cores from the shallowest water depths (RYDER19-8PC and RYDER19-9PC) were collected atop a prominent bathymetric sill lying close to the modern ice tongue calving line (O'Regan et al., 2021). Glaciomarine sediments derive from both clastic and carbonate sedimentary sources (Henriksen et al., 2009; O'Regan et al., 2021). Early Holocene retreat of Ryder Glacier from the fjord mouth, as well as late Holocene retreat following a glacial readvance, coincide with periods of warmer Arctic air temperatures (Levcavalier et al., 2017; O'Regan et al., 2021).

Cores from Thor Iversenbanken in the central Barents Sea were collected from a bathymetric region featuring interconnected basins and channels (Esteves et al., 2022), approximately 15 km from the flow path of the Sentralbankrenna paleo-ice stream (Fig. 1; Bjarnadóttir et al., 2014, Esteves et al., 2017). This basin-channel system is interpreted as a series of paleo-subglacial lake basins located beneath non-streaming ice (Esteves et al., 2022), and sedimentological analyses of cores from this region provide evidence for downstream subglacial meltwater drainage between basins (Esteves et al., 2022). The cores included in our study, CAGE-15-5-1222 and CAGE-15-5-1221, were recovered from within the furthest downstream basin and from a bank adjacent to a basin, respectively (Esteves et al., 2022). The last deglaciation of the central Barents Sea took place at the end of the Pleistocene (e.g., Winsborrow et al., 2010), and supraglacial input to the subglacial hydrological system is inferred from the deglacial landform record (Shackleton et al., 2023). The relict Barents Sea Ice Sheet is heralded as a potential analog for the West Antarctic Ice Sheet because of a submarine ice-sheet base, similar size, and a predominantly sedimentary subglacial substrate (Andreassen and Winsborrow, 2009).

The Marguerite Trough paleo-ice stream drained the Antarctic Peninsula Ice Sheet from the modern coastline over nearly 400 km to the continental shelf break during the Last Glacial Maximum (LGM) ca. 20 ka (Fig. 1; Ó Cofaigh et al., 2014). Geomorphic evidence of ice streaming, a paleo-subglacial channel network incised into bedrock, and remarkably deep (900 m) connected basins are preserved on the deglaciated continental shelf (Ó Cofaigh et al., 2005; Anderson and Fretwell, 2008; Livingstone et al., 2013). Cores in this study were recovered from within moderately deep basins (650-726 m; Table A1) to the west of Marguerite Trough (Kennedy and Anderson, 1989). The tills sampled for this study feature a

	N. Hemisphere		Antarctica			
	Ryder	*TI*	*MTIS*	PIG	TG	Ross
Location		Svalbard Norway				
Subglacial Geology						
Meltwater Source(s)						
LGM Catchment Size						

Subglacial Geology

Hard bed

Soft bed

Meltwater Sources

Glacial
strain heating, pressure melt

Elevated geothermal heat flux

Supraglacial input

LGM Catchment Size

$> 10^6$ km^2

10^5 km^2

$\leq 10^4$ km^2
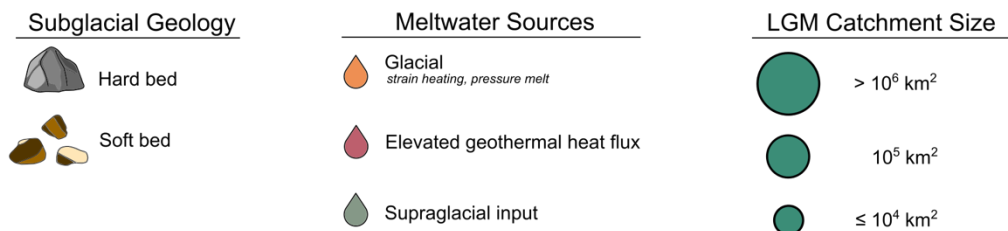
Figure 1. Graphical map illustrating components within a glacial catchment that may influence grain-shape alteration and meltwater production compared between study sites. Subglacial geology is binarized into either hard (i.e., crystalline bedrock) and soft (clastic or sedimentary) beds. Relict glacial catchments and deglaciated setting names are italicized. TI = Thor Iversenbanken, MTIS = Marguerite Trough Ice Stream, PIG = Pine Island Glacier, TG = Thwaites Glacier, Ross = western Ross Sea, LGM = Last Glacial Maximum.

sand-rich (~40 %) matrix material and mineralogy consistent with a quartz- and mica-bearing metamorphic source. The

135 MPDs are rich in silt-sized quartz and feldspar grains (Kennedy and Anderson, 1989). Cores recovered from Marguerite Trough often contain several meter-thick units of diatomaceous and organic-rich sediments. The samples examined in this study, however, were taken from MPD units barren of siliceous microfossils to ensure the grain-shape measurements reflect glaciogenic, rather than hemipelagic, sediments. Initial retreat of the Marguerite Trough paleo-ice stream occurred coeval with Meltwater Pulse 1a at approximately 14 ka (Kilfeather et al., 2011).

140 Thwaites and Pine Island glaciers drain into the eastern Amundsen Sea Embayment today and had coalesced during the LGM, when they advanced to the outer continental shelf (Fig. 1; Kirshner et al., 2012; Larter et al., 2014 and references therein). Post-LGM retreat occurred stepwise across Pine Island Trough until the grounding lines of Pine Island and Thwaites glaciers had stabilized within ~100 km of their current positions by ~10 ka (Hillenbrand et al., 2013; Nitsche et al.,

2013; Witus et al., 2014; Lepp et al., 2022). Cores used in this study (Table A1) were collected on the mid- and inner shelf from a variety of bathymetric settings, including atop a bedrock high that was a former pinning point for the Thwaites Glacier Tongue (Hogan et al., 2020b) and on a ridge beneath the Pine Island Glacier Ice Shelf (Smith et al., 2017). Volcanic and plutonic rocks, largely felsic in composition, underlie the Pine Island and Thwaites glaciers (Smith et al., 2013; Schroeder et al., 2014; Simões Pereira et al., 2020). Additionally, large sedimentary basins upstream have been identified by aeromagnetic surveys (e.g., Muto et al., 2016) and inferred by observations of kaolinite-rich sediments offshore (Hillenbrand et al., 2003; Ehrmann et al., 2011; Simões Pereira et al., 2020). Geothermal heat flux is elevated in the region which likely influences subglacial meltwater supply (Damiani et al., 2014; Schroeder et al., 2014; Dziadek et al., 2021).

Cores collected from the western Ross Sea were recovered from bank tops (NBP1502 KC22; Halberstadt et al., 2018) and from topsets and toes of grounding-zone wedges (NBP1502 KC17, KC19; Prothro et al., 2018) in water depths ranging from 354-549 m (Fig. 1; Table A1). At the LGM, the East Antarctic Ice Sheet occupied the western Ross Sea (e.g., Anderson et al., 2014). However, unlike the other described glaciated regions, the seafloor geomorphology indicates that grounded ice did not extend to the continental shelf break (Greenwood et al., 2012; Halberstadt et al., 2016). High geothermal heat flux is inferred for the western Ross Sea (Simkins et al., 2017) based on the proximity of core sites to volcanic seamounts (Rilling et al., 2009), a rifting zone (Cooper et al., 1987), and heat flow measurements (Blackman et al., 1987 and references therein). Compositionally, the sand fraction of tills from this region consists mainly of felsic lithic fragments (Licht et al., 2005).

2 Materials and Methods

A total of 49 sediment samples from MPDs, subglacial tills, and grounding-zone proximal diamictons from the regions described in Section 1.1 were gathered for this study (Fig. 1; Table A1). For Thwaites Glacier, from which subglacial till was unavailable, MPD grains were compared against grains sampled from grounding-zone proximal diamicton (Table A1). For Pine Island Glacier, where both subglacial till and grounding-zone proximal diamicton were available, we compared MPD grains against all diamicton grains, merging grains from both subglacial and grounding-zone proximal deposits. Subglacial tills and grounding-zone proximal diamictons differ in their depositional environments and processes, but their composition is nearly identical (e.g., Licht et al., 1999). The grounding-zone proximal diamictons included in this study are mainly mass flow deposits that were directly sourced from subglacial till and deposited within just a few kilometers of this grounding zone (Smith et al., 2019). As a consequence, both sediment types are very similar and, in continental shelf settings, virtually indistinguishable (Kurtz and Anderson, 1979). Importantly, the sediment transport processes responsible for grain-shape alteration in the subglacial environment are largely the same prior to deposition. Such subglacial sediment transport processes, like grain rotation, abrasion, and grinding (Benn et al., 2006) are also distinctly different from sediment mobilized in suspension or by saltation via subglacial meltwater. Incorporating materials from both

175 subglacial till and grounding-zone proximal diamicton for comparison with MPDs is therefore appropriate to address questions of grain micromorphological alteration through subglacial hydrological transport.

To further understand how grain micromorphology is altered through subglacial and hydrological transport, we incorporate a spectrum of reference materials. These reference materials include basal ice sediments recovered from Siple Dome in the Ross Sea drainage sector of West Antarctica, fringe debris (i.e., sediment entrained into basal ice through

180 infiltration of ice into sediment pore spaces; Rempel, 2008; Meyer et al., 2019) from Pope Glacier in the eastern Amundsen Sea Embayment, and supraglacial terrigenous and biogenic debris (i.e., cryoconite) from Qaanaaq Glacier in Northwest Greenland. These reference sediments underwent the same suite of analyses and are used to contextualize the micromorphologies observed in our primary sample populations (Table A1).

Subsample from OSO09-10 KC04 3-4 cm
5 microns
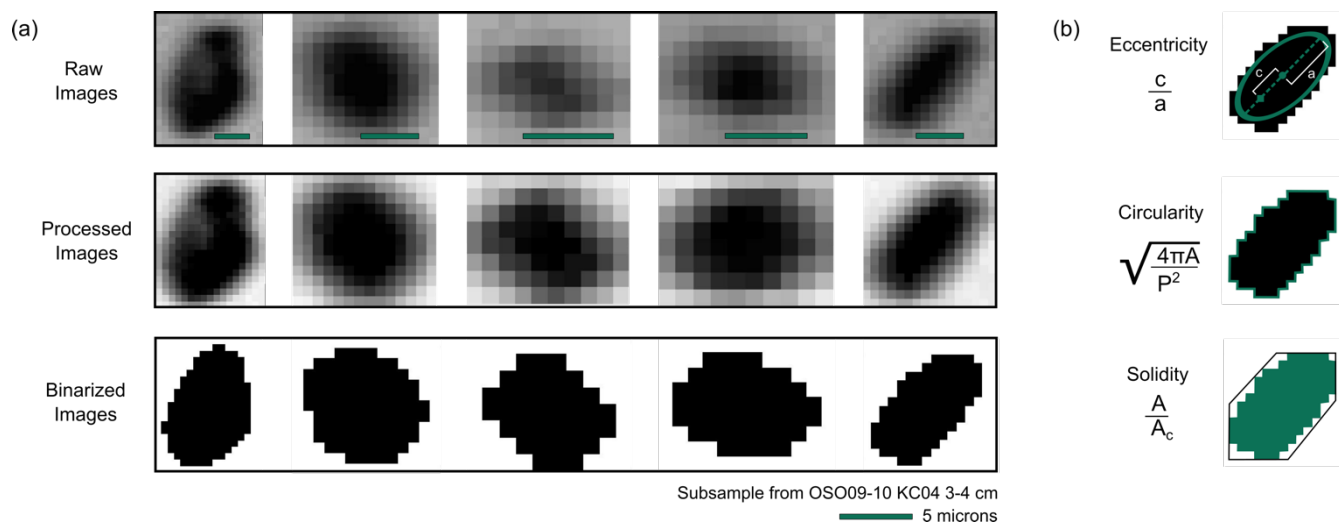
185

Figure 2. Workflow for automated grain-shape analysis. (a) Raw images captured by the Bettersizer S3 Plus, images post-processing, and in binarized forms. (b) Metrics and associated equations calculated for each grain. c = distance between foci and center of an ellipse with the same second-moment as the grain; a= length of semi-major axis; A = grain area, P = grain perimeter, A_c = area of the convex hull, or a simple polygon, that encompasses the grain. The convex hull is illustrated by the black line around the grain.

2.1 Grain-shape analysis

Grain-shape analysis was conducted on all primary and reference samples (Table A1). Bulk sediments were treated with sodium metaphosphate to deflocculate clays for 48 hours prior to analysis. All sediment samples except for MPDs were

190 sieved at 500 microns (μm) to isolate matrix material (Prothro et al., 2018). To remove organics from cryoconite, samples were placed in a hot water bath at 100 °C and 15 % H_2O_2 was added in 1 mL increments until at least two hours elapsed with no observable reaction (adapted from Leidman et al., 2020). While it is possible for glaciomarine sediments containing organics to be reworked into till and grounding-zone proximal diamicton and for organics to be found within MPDs, prior

studies of the samples used here report that organics and other biogenic components are either absent or occur in trace amounts only (e.g., Kennedy and Anderson, 1989; Prothro et al., 2018; O'Regan et al., 2021; Lepp et al., 2022; Clark et al., 2024). Therefore, H_2O_2 treatment was not applied to any core samples. Aliquots of sediment from a homogenized slurry were introduced into a Bettersizer S3 Plus sampling reservoir where grain size was measured through laser diffraction (Lepp et al., 2022). Thousands of images of grains from the same aliquot were subsequently captured for shape analysis using the integrated microscope charge-coupled device cameras with objectives of 0.5x and 10x. Images captured with the 10x objective were exported because this magnification preferentially captures finer grain sizes, including the silt-sized range dominant in MPDs, compared to the 0.5x objective. The lower detection limit for the 10x objective is 0.8 µm; to avoid sampling bias skewed towards that threshold or towards clay minerals, images of grains finer than 2.4 µm were excluded from analysis (Crompton et al., 2019).

A MATLAB script for grain-shape analysis (Lepp et al., 2023; see Data Availability section) randomly selected 200 unique images from each sample, processed images to distinguish foreground from background, converted images from grayscale to binary, and calculated three dimensionless metrics on the binarized shapes using the "regionprops" function (Fig. 2; Vlieghe et al., 2014). The metrics considered included eccentricity, circularity, and solidity, and collectively provide information about grain form (i.e., roundness) and shape (regularity). Evaluating distinct shape metrics, rather than harmonic ranges or grain roughness as employed by other works (e.g., Wellner et al., 2011; Livsey et al., 2013; Witus et al., 2014; Charpentier et al., 2017), allows us to consider the magnitude of variability for each parameter within the context of the other measurements. To test the null hypothesis that grain shapes found in MPDs and subglacial/grounding-zone proximal diamictons from the same glacial catchments are indistinguishable, we performed a two-tailed Z-test on the means of each group for each shape metric considered (probability $p < 0.05$). We calculate 95 % confidence intervals from 1,000 bootstrap replicates for those samples and metrics showing statistically significant differences in means.

2.2 Microtexture analysis

On the basis of the quantitative grain-shape output, some glacial catchments indicated grain-shape alteration of MPDs, and others did not. Accordingly, we selected a subset of samples from both catchment types for scanning electron microscope (SEM) imaging and microtexture analysis. Previous SEM studies on glaciogenic sands (63 µm – 2 mm) have isolated grains through sieving and random grain picking (e.g., Curry et al., 2009; St. John et al., 2015; Passchier et al., 2021). This approach is not suitable for the silt-sized grains of interest here (2 – 63 µm), so the following method was designed to isolate and mount a representative subsample of grains for imaging. For each sample, an aliquot of deflocculated sediment was pipetted from a homogenized slurry and dispensed onto a 63 µm sieve. The fraction that passed through was collected onto a piece of weighing paper. Once dried, a section of the weighing paper was mounted on a sample stub, sputter coated (Au-Pd), and imaged using an FEI Quanta 650 field-emission gun in high vacuum mode. We followed the traditional approach to microtexture analysis, whereby quartz grains are targeted because of their prevalence across depositional

environments and their mineralogical resistance to weathering (Vos et al., 2014). Grain composition was verified as quartz through the Oxford AZtec energy dispersive x-ray spectrometer program prior to imaging.

Grains were categorized according to relief (high to low, following Mahaney, 2002) and roundness (angular to rounded, after Vos et al., 2014). We chose a suite of microtextures, including some associated with glacial transport (cf. Passchier et al., 2021) and others with fluvial transport (cf. Vos et al., 2014; Křížek et al., 2017), and evaluated each grain for presence or absence of these textures to calculate microtexture frequency of occurrence in each sample (Fig. 3). The mean frequencies of occurrence for each microtexture are calculated by sample type (i.e., MPD or till/grounding-zone proximal diamicton), and percent overrepresentation is considered to be the difference between those mean frequencies. Microtexture identification primarily followed Mahaney (2002) who describes microtextures on sand-sized grains by appearance and by size. Yet, because this commonly used reference does not examine silt grains, identification of textures on our samples were based on appearance rather than the specified size scale. For example, Mahaney (2002) describes arcuate and straight steps as microtextures that occur on the scale of > 5 µm. However, these textures were visually identified on silt grains imaged in our study (Fig. 3) and are found to occur at finer scales than described by Mahaney (2002).

3 Results

3.1 Grain-shape distributions

Of all metrics considered, eccentricity shows the greatest statistical variance between glacial catchments. The standard deviation for the median eccentricities of all MPDs is 3.4 %, whereas it is 4 % for all samples from subglacial till or grounding-zone proximal diamicton (Fig. 4). Grains of both populations from the Marguerite Trough Ice Stream encompass the widest spread of eccentricities for all regions considered, with an average interquartile range of 0.25. Thor Iversenbanken and Marguerite Trough samples contain grains that are generally more eccentric relative to the other four catchments. In the other four catchments (Ryder Glacier, Thwaites Glacier, Pine Island Glacier, and the western Ross Sea) distributions of eccentricity for both grain populations are strikingly similar with interquartile ranges from 0.38 to 0.66 (Fig. 4), though the median eccentricity for Thwaites Glacier grains is slightly elevated at 0.53. The Marguerite Trough Ice Stream is the only catchment where the difference in eccentricities of MPD and till grains is highly significant, with grains from the MPD being less elongate than grains in the till. Eccentricities of MPD and till grains from Pine Island Glacier were found to be significantly different, again with MPD grains being less elongate (Table A2).
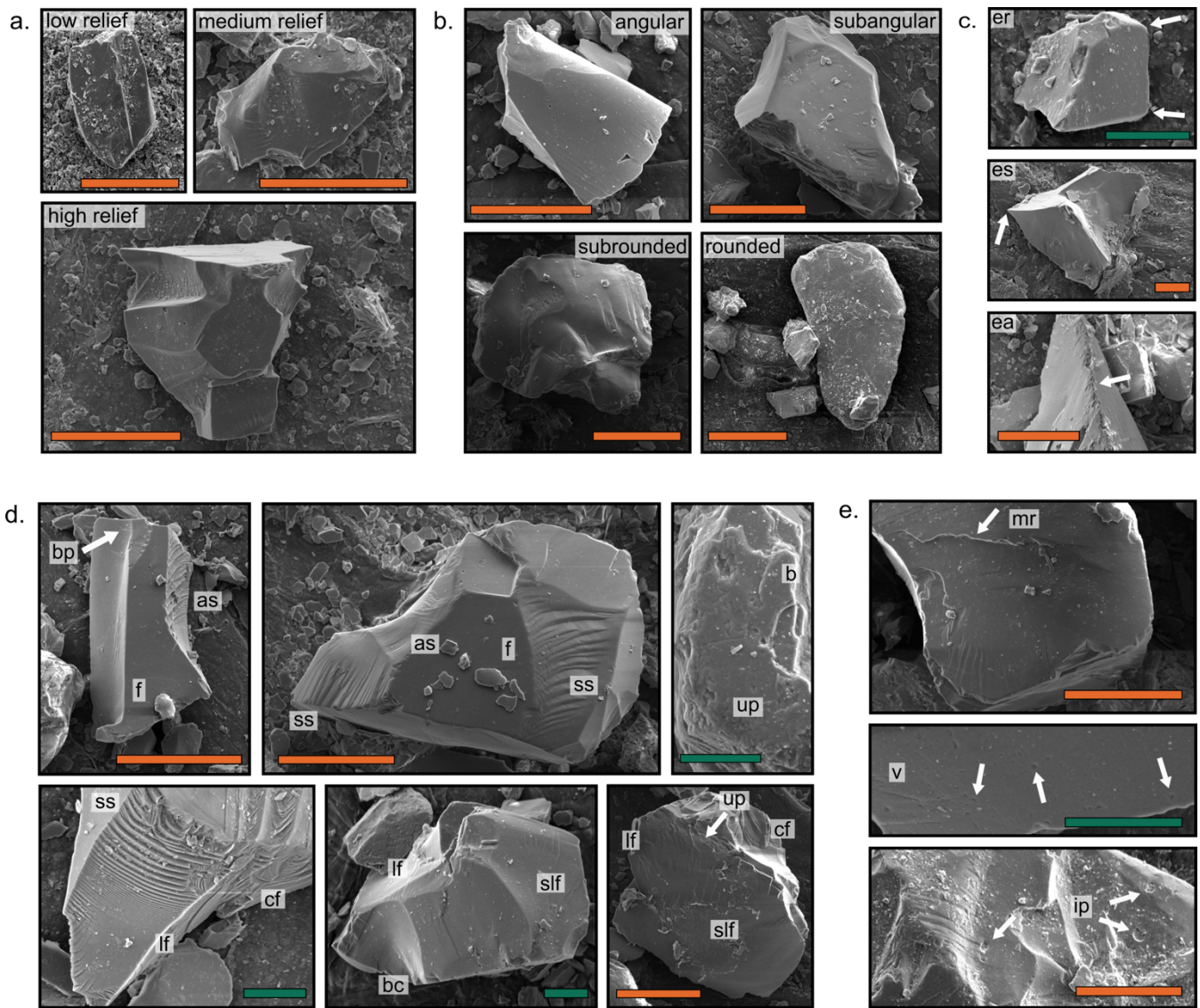
Figure 3. Microtextures observed on silt-sized quartz grains in the <63 μm size fraction from selected samples of subglacial till and meltwater plume deposits. Orange scale bar = 20 μm. Green scale bar = 5 μm. (a) Grain relief and (b) grain shape, following Mahaney (2002) and Vos et al. (2014), respectively. (c) Edge characteristics. (d) Fracture types characteristic of glacial transport, following grain types B-D from Passchier et al. (2021). Note the differences in scale bars. (e) Microtextures associated with fluvial transport, following Křížek et al. (2017). as = arcuate steps, b = breakage block, bc = breakage concavity, bp = broken plates, cf = conchoidal fracture, ea = edge abrasion, er = rounded edges, es = sharp edges, f = fracture face, ip = impact pit, lf = linear fracture, mr = meandering ridges, slf = sublinear fracture, ss = straight steps, up = upturned plates, v = v-shaped percussions.

255   On average, the most circular grains are found in MPDs from the western Ross Sea (mean: 0.63, median: 0.64)

while the least circular grains are found in tills from the Thor Iversenbanken (mean: 0.55, median: 0.56). An intercomparison

of circularity data for MPDs from all catchments, with the addition of plume deposit data from three glacial catchments

260 (without till samples), reveals modest variability between interquartile range for all MPDs (0.51-0.69) with no clear regional trend (Fig. 5). MPD grains from Marguerite Trough are less circular than those from other

265 Antarctic deposits and have interquartile ranges similar to those of MPD grains from the Barents Sea (Thor Iversenbanken and Kveithola) and the Nares Ice Stream (Fig. 5). Ryder Glacier and Petermann Ice Stream

270 MPD grains have the widest interquartile ranges, with median values resembling samples from Pine Island Glacier and the western Ross Sea, respectively. We also note that the circularity distributions for MPD

275 grains from all catchments overlap with one another and are largely confined between values of 0.4 and 0.8 (Fig. 5). For all six regions, the median circularity of MPD grains is higher than that of the grains in the

280 corresponding subglacial tills, but differences in means are significant only for Ryder Glacier, Pine Island Glacier, and western Ross Sea samples (Fig. 4). Interestingly, interquartile ranges for MPDs from

285 Marguerite Trough Ice Stream and Thwaites Glacier do not show enhanced circularity relative to grains from source tills or grounding-zone proximal diamictons. Instead, these MPDs appear to
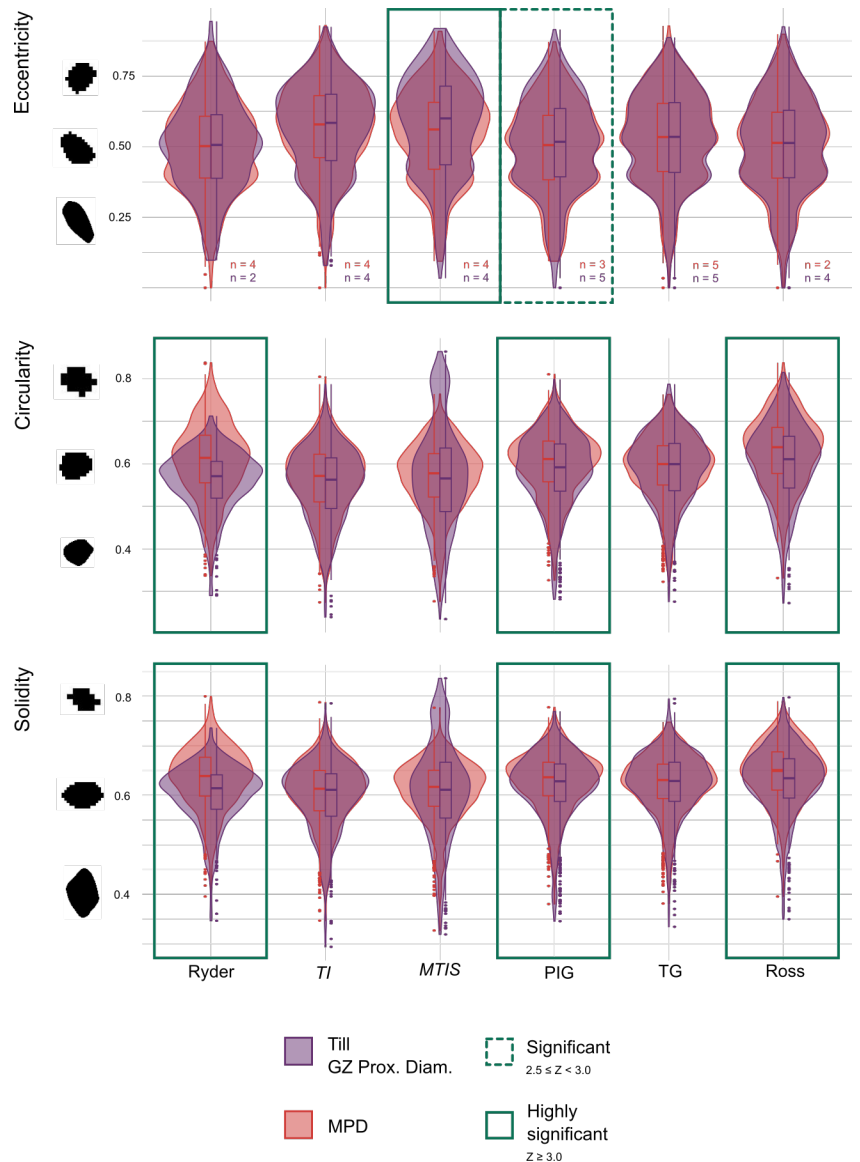
Figure 4. Violin plots for paired MPDs and tills, or grounding-zone proximal diamictons (GZ-Prox. Diam.; Table A1), for each region with the number of samples from each grain type shown at the bottom of grain eccentricity. Box plots within each violin show the interquartile ranges. Those pairs outlined in solid green denote populations that are highly significantly different, while the dashed green line indicates pairs that are significantly different as determined by a two-tailed Z test. Refer to Fig. 2 for shape metric equations. TI = Thor Iversenbanken; MTIS = Marguerite Trough Ice Stream, PIG = Pine Island Glacier, TG = Thwaites Glacier, Ross = western Ross Sea.

11

comprise grains with restricted subsets of circularities that overlap with corresponding source grain samples (Fig. 4).

Solidity describes regularity of grain perimeters. The median solidity for till grains from Ryder Glacier, Thor Iversenbanken, and Marguerite Trough is 0.61, whereas that for till grains from Pine Island Glacier, Thwaites Glacier, and the western Ross Sea are slightly higher (0.628-0.634). As with circularity, MPD grains from Marguerite Trough and Thwaites Glacier exhibit narrower interquartile ranges of solidities than grains in corresponding subglacial sources. Consequently, the mean and median distribution for each grain population is

Figure 5. Circularity of meltwater plume deposit grains with first and third quartiles indicated by dashed lines and the median by a solid line. Glacial catchments are grouped and colored by region. Samples with no till counterpart are denoted by ^ (see also Table A1).

virtually the same for these glacial catchments. The interquartile ranges for Ryder Glacier, Thor Iversenbanken, Pine Island Glacier, and the western Ross Sea demonstrate shifts to enhanced grain regularity from subglacial tills to MPDs, with those differences being highly significant for all but the Thor Iversenbanken (Fig. 4).

We acknowledge that grain size, and therefore image resolution (Fig. 2), may have some influence on the observed grain-shape distributions. However, none of the distributions for any metric considered are strongly skewed towards upper or lower limits as we would expect if image resolution was controlling the distribution of shape values. These results suggest that the preventative measures integrated into the methodology (removing grains below 2.4 μm; random selection of grains to use in analysis) sufficiently removed any grain-size bias from the grain-shape results.

3.2 Microtexture observations

A total of 63 grains were imaged from four MPDs and 69 grains were imaged from four till/grounding-zone proximal diamictons (Table A1). For the same purposes as outlined in the Methodology, we interpret the microtextural data from a grounding-zone proximal diamicton (Table A1) together with that from the subglacial till samples. Imaging was attempted on nearly twice as many samples as are presented on here, but the fine-grained and electrostatic nature of MPDs posed challenges for isolating silt-sized quartz grains. Many samples imaged were dominated by clays and had fewer
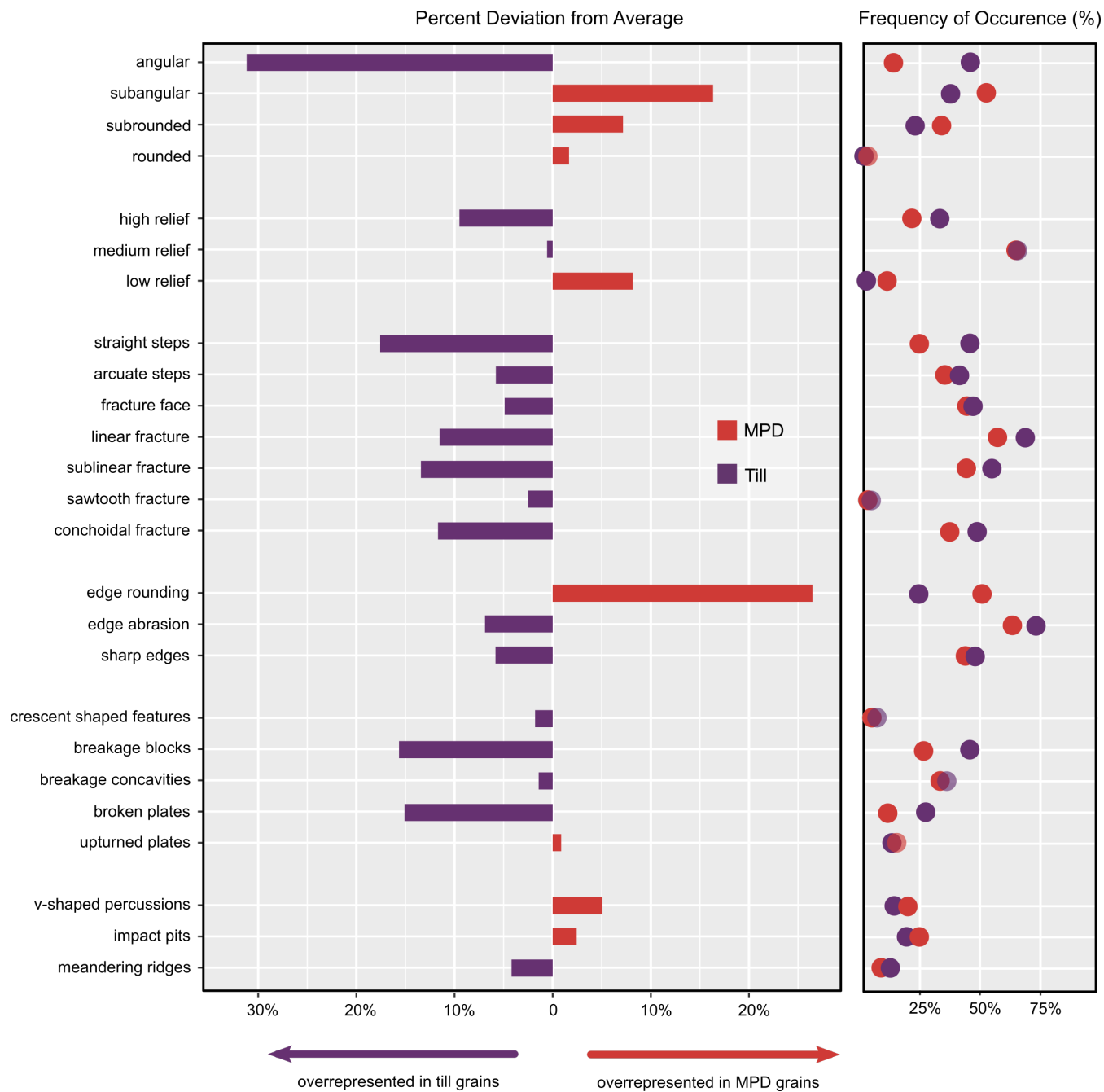
Figure 6. Overrepresentation and frequency of occurrence of microtextures on 132 quartz grains from tills and MPDs (for examples of microtextures, see Fig. 3). Angular grains and all fracture types, as well as edge abrasion, are overrepresented in till grains, whereas MPDs exhibit a higher proportion of subangular and subrounded grains with edge rounding. Many mechanical microtextures (e.g., fracture faces, linear and sublinear fractures) are observed at comparable frequencies in both grain populations.

than 10 quartz grains. The eight samples included in microtexture observations imaged between 12 and 20 quartz grains each, which is within the range considered to be representative for any given SEM sample (cf. Vos et al., 2014).

325 At the micron to sub-micron scale, microtextures characteristic of glacial transport are visible on quartz grains (e.g., Fig. 3d) in all grain populations, demonstrating that microtexture analysis on glaciogenic silts is both feasible and provides meaningful data. Angular grains and grains with high relief are found to be overrepresented in subglacial till samples compared to MPDs by 31 % and 10 %, respectively (Fig. 6). Conversely, grains with subangular and subrounded shape, as well as low relief grains, occur in higher abundance in MPDs (Fig. 6). Regardless of sample type, round grains are comparably rare and grains with medium relief are the most abundant relief type (Fig. 6). All step and fracture textures that

330 are attributed to high stress, grinding, plucking, and abrasion in glacial environments (Vos et al., 2014; Passchier et al., 2021) are overrepresented in till grains, ranging from 3 % (sawtooth fractures) to 18 % (straight steps) more common than in MPD grains (Fig. 6). Additionally, breakage features, such as blocks, concavities, and plates, are observed in moderate (≤ 50 %) abundance in all grain types and are overrepresented in tills.

Fluvial microtextures imparted to grain surfaces through intergranular collisions during transport in suspension are

335 observed on both till and MPD grains, but with abundances ≤25 % are not pervasive features (Fig. 6). V-shaped percussion cracks and impact pits are overrepresented in MPD grains by only 5 % and 2 %, respectively, whereas meandering ridges are, somewhat surprisingly, overrepresented by 4 % in till/grounding-zone proximal diamicton grains. Notably, grains in MPDs exhibit edge rounding 26 % more often than is observed in till and grounding-zone proximal diamicton samples. Although differences in average frequencies allow us to compare microtexture abundance between tills and MPDs, nearly all

340 textures are observed in some abundance in each grain population. Overrepresentation of a suite of textures in one grain type does not, therefore, reflect absence, or even low abundance, of that feature in the other grain type. Edge abrasion and linear fractures, for example, are both overrepresented in till grains, but are seen on over 50 % of grains in both till and MPD samples.

4 Discussion

345 We find that significant differences in grain shape exist between MPDs and tills in some regions, as well as between MPDs from different regions, and that those differences can be both quantified using an automated imaging approach and, generally, verified qualitatively with microscopy. Here, we consider potential reasons for those variations and discuss implications for subglacial sediment transport processes, with an emphasis on subglacial hydrology.

4.1 Widespread subglacial sediment transport processes

350 Despite the differences in subglacial bed composition, drainage basin size, glacial histories, and source(s) of basal meltwater for the various glacial catchments (Fig. 1), we find that three-quarters of all grains studied can be described by approximately one-quarter of possible grain morphologies, alluding to highly efficient and ubiquitous erosive processes that

likely operate on catchment-wide scales. Through these processes, grains with extreme morphometries (i.e., highly elongated/rounded, or highly irregular/regular) are either not produced in abundance or such extreme grain shapes are

355 maintained for a short time only. Variability in grain micromorphology between glacial catchments likely reflects differences in subglacial substrate geology and mineralogy, glacial history (i.e., reworking and textural maturity of sediments), distance of transport, volume of meltwater present, or some combination of these factors (Fig. 1).

Our dataset suggests that although regional mineralogy may explain some variation in grain shape, it is insufficient to explain all observed differences in grain-shape distributions. In NW Greenland, for example, circularity of MPD grains is

360 not identical for all glacial catchments despite similar catchment areas and meltwater sources (Figs. 1, 5). Mineralogically, Petermann Glacier detritus contains abundant calcite and dolomite (Jennings et al., 2022), while Nares Ice Stream detritus is enriched in quartz and micas (Jennings et al., 2022). Ryder Glacier detritus consists of both carbonate and clastic sedimentary components (O'Regan et al., 2021) and shows an interquartile range of grain circularity between the other two catchments, suggesting mineralogical differences can manifest in grain-shape variability when glacial and climactic

365 conditions are comparable. Yet, circularities of MPD grains from NW Greenland and West Antarctica are quite similar (Fig. 5), despite glacial catchments in the latter having larger drainage basins, experiencing less supraglacial melt, and lacking carbonate sedimentary substrates (Fig. 1; Section 1.1). Furthermore, subglacial till grains from Ryder Glacier are more irregular than those from West Antarctic glaciers (Fig. 4), alluding to impacts on MPD grain shape unrelated to substrate geology. Of the metrics considered, eccentricity is likely to be most sensitive to mineralogy as this would capture differing

370 proportions of equant and elongated, or platy, minerals (e.g., Marsaglia et al., 2013). Yet, median eccentricity for all MPD grains varies by only ~8 % between glacial catchments (Fig. 4), further demonstrating that source rock alone does not fully explain all variation in the dataset.

When we consider the grain-shape distributions for supraglacial debris, basal ice debris, and frozen fringe debris in relation to subglacial tills and MPDs from the studied regions, the erosive power of subglacial sediment transport becomes

375 abundantly clear (Fig. 7). Circularities of supraglacial cryoconite grains from Qaanaaq Glacier, NW Greenland are very different (Z >>> 3) from grains in subglacial tills from neighboring Ryder Glacier (Fig. 7a). The same is true for basal ice debris from Siple Dome, West Antarctica, and subglacial tills collected offshore from the adjacent Ross Ice Shelf (Fig. 7e). Both the supraglacial debris and the englacial basal detritus (from a stagnant ice dome) represent sediments that are completely or relatively unaltered by subglacial transport. For the ice dome debris, ice advection and subglacial sediment

380 transport are expected to be minimal when compared to basal ice debris from beneath ice streams or at ice margins (e.g., Knight et al., 2002; Christoffersen et al., 2010). In the eastern Amundsen Sea Embayment, the grain-shape distributions for subglacial till and grounding-line proximal diamicton from Pine Island and Thwaites glaciers are less distinguishable from the reference material, frozen fringe debris from neighboring Kay Peak, Pope Glacier (Fig. 7c, d). Sediment entrainment, transport, and release from a frozen ice fringe depend on the thermal and pressure conditions of basal ice (Rempel, 2008;

385 Iverson et al., 2017) and is spatiotemporally transient. For that reason, it is likely that debris from this till fringe has undergone transport processes at the ice-bed interface prior to fringe entrainment, unlike grains from cryoconite and basal ice

debris (e.g., Iversen et al., 2017). Therefore, it can be expected that the circularities of subglacial till grains differ more from those of supraglacial or basal ice debris grains than from those of grains from fringe ice debris. Our results are consistent with this expectation (Fig. 7).

The added context gleaned by examining micromorphology of grains that have undergone little to no subglacial transport (cryoconite and basal debris from an ice dome) indicates that all grains from MPDs, subglacial tills, and grounding-zone proximal diamictons in this study experienced shape alteration through subglacial sediment transport processes. Processes like grain rotation and grinding occur predominantly in dilatant, deforming tills (Evans et al., 2006; Robinson

Figure 7. Grain-shape evolution. (a), (c), and (e) show grain circularity for grounding-zone proximal diamicton (GZ-Prox. Diam), subglacial till, and meltwater plume deposits in comparison to supra- or englacial reference material from a neighboring glacial catchment. SEM images of (b) supraglacial cryoconite, (d) basal fringe debris, and (f) englacial debris from the base of an ice dome. Note that in (c) the middle violin includes samples from grounding-zone proximal diamicton offshore Pine Island and Thwaites glaciers, as well as subglacial till samples from Pine Island Glacier (Table A1). Scale bar in (b), (d), and (f) is 20 microns.

et al., 2021) that are associated with high basal water pressures and streaming of glacial ice (e.g., Boulton et al., 2001; Evans et al., 2005; Reinardy et al., 2011; Rüther et al., 2012). Thus, this finding suggests most grains in our study underwent some degree of subglacial transport, and a subsequent increase in measurable roundness and regularity, beneath fast-flowing ice. Such ice streaming conditions have similarly been inferred from other paleo-subglacial records, such as subglacial bedforms and till properties, in the studied regions (Nitsche et al., 2013; Esteves et al., 2017; Jakobsson et al., 2018; Munoz and
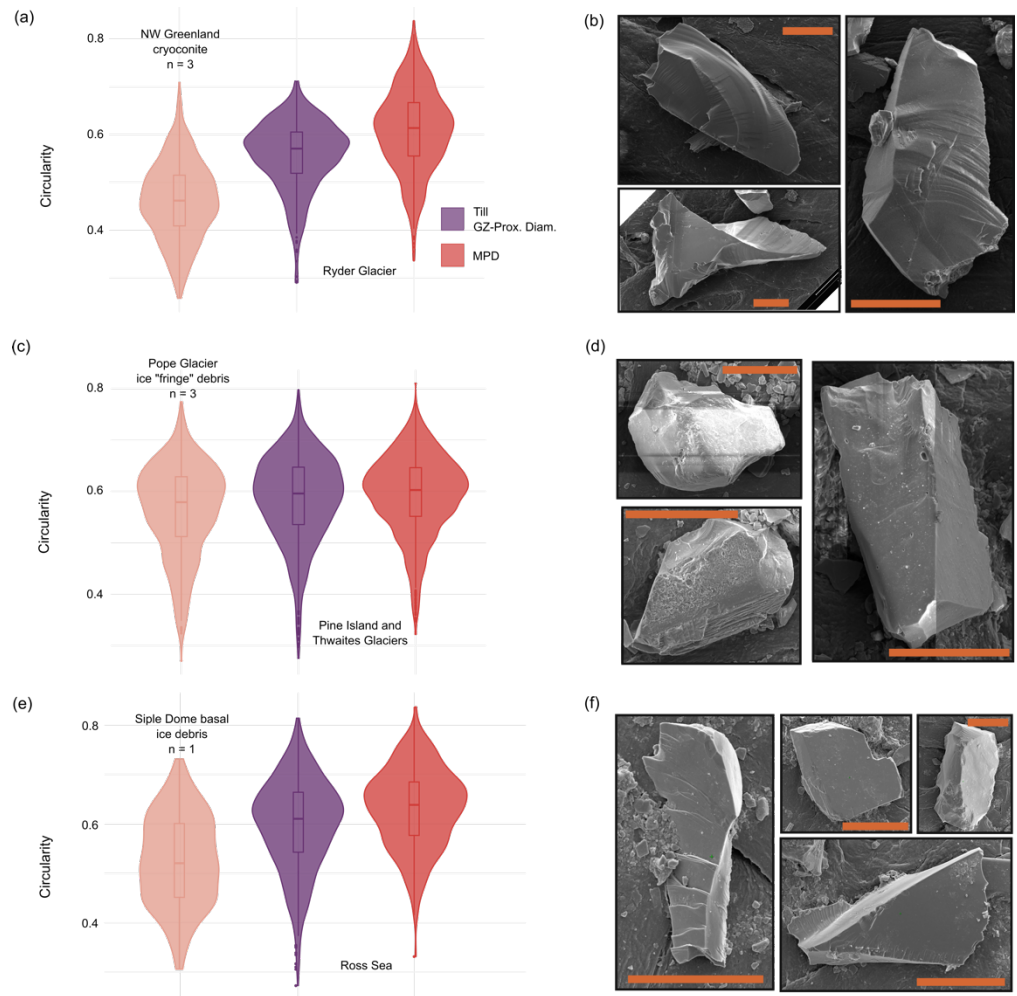
Wellner, 2018; Simkins et al., 2018; Kirkham et al., 2019, 2020; Hogan et al., 2022). However, no geomorphic evidence of ice streaming exists on Thor Iversenbanken (Esteves et al., 2022). Instead, MPD and subglacial till grains from this area may have experienced morphological alteration through shearing or brittle deformation (e.g., Evans et al., 2006) that produced a slightly more irregular, elongate grain-shape signature (Fig. 4).

425   The observed general homogeneity in grain morphology may reflect the lasting impact of grain cushioning, whereby fine grains fill interstitial spaces between larger till clasts and, through grain rolling, act to absorb and dissipate tensile stresses along grain bridges (Iverson et al., 1996; Menzies, 2012; Robinson et al., 2021). This effect has been shown to produce a self-similar grain-size distribution (Iverson et al., 1996), and it is possible the same may be true for grain shape. The volume of subglacial meltwater influences how grains through a till column will be mobilized and therefore indirectly

430   affects grain-shape alteration through the processes discussed above. Yet, the restricted grain morphometries across all sites coupled with the significant differences in grain morphometry between subglacial till grains and glacial grains with limited subglacial transport suggest subglacial sediment transport is chiefly responsible for producing the observed, largely homogenous grain shape distributions. We acknowledge, of course, the Sisyphean challenges associated with untangling inherited grain shape from earlier glacial cycles or interglacial subaerial sediment transport (Evans et al., 2006), but do not

435   think our inability to do so detracts from the findings of shape homogeneity for silt-sized grains in tills and MPDs from a geographically-diverse sample population.

4.2 Production of meltwater silts

Subglacial processes responsible for generating glacial silts and the "terminal grain-size mode", or the smallest silt-size to which a grain can be comminuted based on its mineralogical structure, have been explored through field observations

440   and controlled experiments (e.g., Dreimanis and Vagners, 1971, 1972; Iverson et al., 1996; Crompton et al., 2019). These studies have largely agreed that abrasion is a widespread process in subglacial environments (Alley et al., 2019) driving comminution by exploiting weaknesses in the mineral fabric of larger grains (Haldorsen, 1981; Crompton et al., 2019), and that the microtextural signatures of abrasion on grain surfaces include different step and fracture types (e.g., Mahaney, 2002; Passchier et al., 2021). Furthermore, abrasion beneath glacial ice has been credited with rounding grain shape (Hart, 2006;

445   Rose and Hart, 2008), which is consistent with the degrees of solidity and circularity in our results, particularly for those most mature (i.e., undergone reworking by multiple glacial advance and retreat cycles) sediments from West Antarctica (Figs. 4, 5).

We observe microtextures resulting from abrasive processes, including conchoidal fractures, arcuate and straight steps, parallel and sub-parallel fractures, on a large proportion of grains from both MPD and subglacial till samples (Fig. 6).

450   The high abundance of microtextures imparted through sustained stress and grinding (e.g., fracture types, edge abrasion) coupled with the low frequency of fluvial textures (e.g., v-shaped percussions) on both grain populations strongly suggests the grain-size production of the ~10 μm meltwater-silt mode results from abrasion and grinding at the base of glacial ice,

rather than the comminution of grains during subglacial hydrologic transport (e.g., Schroeder et al., 2019). Witus et al. (2014) reached a similar conclusion after examining sand grain microtextures from MPDs and tills collected offshore from Pine Island Glacier (samples which we also include in this study, Table A1). Collectively, our results provide grain-scale evidence in support of the hypothesized subglacial origin of MPDs inferred from shared grain-size modes (Witus et al., 2014; Simkins et al., 2017; Prothro et al., 2018) and geochemical similarities (Lepp et al., 2022) with subglacial till and grounding-zone proximal diamicton.

Although we did not include samples from each study region due to methodological challenges (e.g., insufficient number of silt-sized quartz grains present on a prepared sample stub, adhering clay particles obscuring quartz grain surfaces), we have found meaningful results from the data subset. This study represents, to our knowledge, the first quartz microtextural analysis on the silt grain-size fraction. Microtextural studies of sand grains have advanced our ability to connect the sedimentological record with depositional settings and processes of the past, in glacial environments and beyond (Mahaney, 2002; Cowan et al., 2008; Vos et al., 2014; St. John et al., 2015; Křížek et al., 2017; Passchier et al., 2021). To build on existing knowledge, we encourage future microtextural investigations to include and/or to focus on the silt fraction because its grains provide additional context for glacial histories, sediment transport processes, or paleoclimate reconstructions of glaciated or formerly glaciated regions.

4.3 Subglacial hydrological inferences from grain micromorphology

While the grain-shape distributions of MPDs do not exhibit the same striking similarity as their grain-size distributions (e.g., Witus et al., 2014; Prothro et al., 2018; Jennings et al., 2022; Lepp et al., 2022), we do find that median circularity (Fig. 5) and eccentricity of grains from all investigated MPDs vary by less than 10 % and that distributions overlap with one another. However, because their shape distributions also overlap with those of grains from tills and grounding-zone proximal diamictons, we cannot describe the MPD grain-shape distributions as characteristic for this type of deposit. Similarly, we do not observe pervasive evidence of glaciofluvial transport in surface microtextures on MPDs (Fig. 6). These deposits are described as comprising largely silt and clay with grain-size modes at or below 10 µm (Witus et al., 2014; Prothro et al., 2018; Jennings et al., 2022; Lepp et al., 2022), which is below the lower boundary of the sortable silt fraction where silt particles behave cohesively (10-63 µm; McCave et al., 1995). Fine silts in coastal settings (e.g., Manning et al., 2013) and glacial environments (e.g., Greco and Jaeger, 2020) behave cohesively and will form floccules with clays, which has important implications for plume migration and dispersal of MPDs into the marine environment. Silt floccules in the same size range as MPDs are experimentally shown to be stable in both freshwater and saline conditions at current speeds up to 25 cm s^{-1} (Yawar and Schieber, 2017). In non-outburst style subglacial flows, aggregated meltwater silts would have less exposed surface area onto which intergranular collisions could impart microtextures (Vos et al., 2014). This "aggregate shielding" effect could explain both the paucity of fluvial microtextures and retention of mechanical textures

18

observed on MPDs, and is consistent with inferred episodic, low-magnitude drainage styles offshore from the eastern Thwaites Glacier (Lepp et al., 2022).

Alternatively, sluggish flow conditions and/or short transport distances may suffice to reduce grain relief and round edges but may be insufficient to impart abundant fluvial microtextures (Fig. 6). Microtexture studies on proglacial stream sediments find a positive correlation between transport distance and abundance of fluvial microtextures, but only after downstream transport distances from 3 km (Křížek et al., 2017) to at least 80 km (Sweet and Brannan, 2016). For an evolving or transient subglacial drainage network through which flow is not constant or channelized, grains may be mobilized in suspension for only brief (i.e., sub-kilometer) distances before being deposited or entrained in basal ice via supercooling, where alteration through intergranular collisions is minimal (Alley et al., 1997; Creyts and Clark, 2010; Alley et al., 2019). In the absence of supraglacial input to the bed, such continuous flow over several or tens of kilometers may not be sustained. Rather, grains comprising MPDs experience short "bursts" of energy and entrainment (i.e., during subglacial lake drainage events) or mobilization within a sluggish, lower flow regime (i.e., through water films or distributed drainage) wherein fluvial microtextures are not to be expected (Mahaney, 2002; Sweet and Brannan, 2016). Low energy flow regimes associated with modest grain alteration inferred for sediments from Thwaites Glacier are consistent with stratigraphic inferences from marine sediment cores collected from the Thwaites Eastern Ice Shelf (Lepp et al., 2022; Clark et al., 2024). Conversely, MPDs from other catchments, including Pine Island Glacier and the western Ross Sea, are interpreted to have rapidly accumulated through intensive subglacial drainage events, potentially the result of subglacial lake drainage (Lowe and Anderson, 2003; Kirshner et al., 2012; Witus et al., 2014; Prothro et al., 2018). MPD grains are significantly more regular and rounded than grains from subglacial tills and grounding-zone proximal diamictons in these areas (Fig. 4), which may be the result of intensive, but short-lived, drainage events not recorded in the other glacial settings.

Of all sites considered, the most significant grain-shape alteration between subglacial tills and MPDs is observed in samples from Ryder Glacier (Fig. 4). In some locations, MPDs deposited during early to mid-Holocene retreat of Ryder Glacier are three to over five meters thick (O'Regan et al., 2021) indicating a highly active, well-connected subglacial drainage network coeval with elevated air temperatures and enhanced surface melt production (Levcavalier et al., 2017; McFarlin et al., 2018). Such a drainage configuration and supply of meltwater to the ice bed would likely be capable of transporting water and sediments over long (i.e., 10^1-10^2 km) distances (e.g., Shackleton et al., 2023). Furthermore, subglacial till from Ryder Glacier contains grains with the least regular morphometry of all subglacial samples (Fig. 4). This likely reflects that this till was more recently eroded from subglacial bedrock and has been morphologically altered through far fewer glacial advance-retreat cycles than West Antarctic till samples. Cumulatively, we interpret the enhanced rounding and regularity of Ryder Glacier MPD grains when compared to grains in their subglacial sediment sources to result from the combined presence of younger, less rounded grains in the till source (Fig. 4) and the input of supraglacial melt to the bed, which is most common in temperate glacial conditions. Some catchments in West Antarctica show significant differences in grain solidity and circularity between grain populations, although these differences are of smaller magnitude than for Ryder Glacier (Fig. 4). We therefore infer that meltwater action can alter subglacial till grains to be quantifiably more rounded and

19

regular through continuous sediment entrainment over long distances (i.e., many tens of kilometers) or through high-energy outburst-style flow. A supraglacial supply of meltwater to the bed and younger, less reworked till grains can further enhance the magnitude of alteration in the resultant MPD grains. Conversely, the transport of mature till grains via poorly developed channel networks, sluggish flow, and/or short sediment transport distances may produce MPDs with grains that are similar in roundness and regularity to till grains. Results from Ryder Glacier suggest that a grain micromorphological approach may be able to distinguish MPDs originating from subglacial plumbing networks that received substantial supraglacial input from MPDs sourced from subglacial drainage systems with little or no supraglacial input.

4.4 Subglacial basins as reservoirs and subglacial lake drainage

Model results (e.g., Carter et al., 2011) and satellite observations (Wingham et al., 2006; Fricker et al., 2007; Bowling et al., 2019; Hoffman et al., 2020) indicate subglacial water can be stored in, and actively transmitted between, subglacial basins, demonstrating connected subglacial plumbing that mirrors basin-channel systems preserved on deglaciated continental shelves (e.g., Lowe and Anderson, 2003; Anderson and Fretwell, 2008; Kuhn et al., 2017; Simkins et al., 2017; Kirkham et al., 2019; Hogan et al., 2020b). The importance of subglacial lakes as reservoirs of glacial melt and sediments have been evoked to explain discrepancies between annual production of basal melt and volume of water required to mobilize quantities of MPDs observed offshore (e.g., Witus et al., 2014; Schroeder et al., 2019; Lepp et al., 2022). For example, the distribution of ~120 km^3 of silts deposited offshore from Pine Island Glacier is interpreted to have been sourced in part by high-magnitude purging events of subglacial reservoirs of water and sediments (Witus et al., 2014). Samples from those same silts are included in this study (Table A1), and although we found MPD grains to be significantly more regular and rounded compared to till grains (Fig. 4), neither our study nor Witus et al. (2014) observed abundant fluvial microtextures expected from such high-energy sediment transport.

From our results arise discrepancies between inferences made based on grain surface textures and the shape of MPD grains compared to their subglacial sources, and theories and observations of subglacial hydrologic transport. Such discrepancies prompt a consideration of the extent to which sediments are cascaded (Siegfried et al., 2016; Malczyk et al., 2020; Livingstone et al., 2022) downstream along with meltwater during subglacial lake drainage events. Beneath the contemporary West Antarctic Ice Sheet, flux of meltwater over distances of tens of kilometers between subglacial lake basins has been indirectly observed beneath Thwaites Glacier (Hoffman et al., 2020; Malczyk et al., 2020). Channelized meltwater drainage under modern Thwaites Glacier is inferred to extend to the grounding line from 50 km upstream (Schroeder et al., 2013), yet grain morphologies of MPDs deposited directly offshore from this region suggest discontinuous grain entrainment and sluggish flow (Fig. 4). In the Thor Iversenbanken region of the central Barents Sea, paleo-subglacial channels are discontinuous and connect basins over comparatively short distances of ~3-5 km (Esteves et al., 2022). While no Thor Iversenbanken samples were included in the microtexture analysis in our study, the results of the two-tailed Z test indicate that grain shapes in till and MPDs from this region are statistically the same (Table A2). This observation implies a

550 connection between the distance of sediment transport through subglacial drainage networks and the degree of grain-shape alteration of silts in MPDs. A similar relationship between sediment transport distance and abundance of fluvial microtextures has been inferred from site-specific studies of glaciofluvial sediments (Sweet and Brannan, 2016; Křížek et al., 2017). Drainage between East Antarctic subglacial lakes is recorded over distances an order of magnitude higher than those in Thor Iversenbanken (Wingham et al., 2006), implying that grains from MPDs deposited offshore from the East Antarctic

555 Ice Sheet may show greater morphological alteration from till grains. Recent insights from modern subglacial lake sediments recovered in the Siple Coast region of the Ross Sea drainage sector suggest that silt-sized sediment can indeed be mobilized downstream between basins (Hodson et al., 2016) and cores from subglacial lakes could represent a high-resolution record of drainage activity (Siegfried et al., 2023). However, we infer from the modest microtextural evidence of fluvial transport, such as v-shaped percussions and meandering ridges, that a continuous, downstream transport of glacial silt through

560 subglacial plumbing networks enroute to the ocean is unlikely. Grain micromorphology indicative of subglacial transport through till deformation, such as edge abrasion, steps, and various fracture types, is dominant even in MPDs. This dominance, coupled with only minimal overprint of fluvial or meltwater features, renders sediment transport through subglacial plumbing networks over large areas or for extended periods unlikely, even though the final mode of transport and grain sorting may be via subglacial meltwater (cf. Simkins et al., 2023).

565 **5 Conclusions**

Quantitative grain shape and microtexture analyses demonstrate that the shape of silt grains abundant in MPDs can record alteration by subglacial meltwater action from their till origins. By calculating grain shape metrics on thousands of grains from six different glacial catchments, we find that 75 % of grains can be described by approximately 25 % of possible grain circularities, solidities, and eccentricities. This homogenization of grain shape provides evidence for efficient grain

570 comminution and transport through glacial processes that operate at the catchment-wide scale. We find that MPD grains preserve surface textures diagnostic of sustained stress and subglacial grinding but only modest evidence of fluvial transport. This indicates that glacial processes, including abrasion, are responsible for producing the grain-size fraction that comprises MPDs from the glacial catchments we studied. In general, the alteration of grain micromorphology through hydrologic transport is recorded more prominently by edge rounding and enhanced grain regularity than by imparting of surface

575 textures. We suggest this may be due to an aggregate shielding effect and discontinuous transport distances and processes that are insufficient to leave a pervasive microtextural mark. Regional geology, glacial history, and catchment size may exert some influence on regional variability in grain-shape distributions. However, the grain shape data cumulatively suggest that the greatest grain-shape alteration occurs as a result of high-magnitude, outburst-style drainage events or when subglacial meltwater flux is partly supplied by supraglacial input. Additionally, grain-shape alteration via subglacial drainage may be

580 more pronounced when subglacial till grains are more irregular in shape and texturally "younger" (i.e., they have been subglacially reworked over only a few glacial cycles). Grain micromorphology can be a valuable addition to traditional

21

glacial and glaciomarine sediment analyses, especially when a highly active subglacial drainage network is expected (i.e., due to the input of substantial supraglacial melt to the ice bed). Further, we encourage combined empirical and experimental studies that incorporate grain micromorphology to quantifiably connect grain-shape alteration with transport distance to

585 better understand realistic subglacial sediment transport pathways to the ocean.

Appendices

Table A1: Sample identification, coordinates, water depth, facies, associated glacial catchment or region, and reference for all samples used in this study. Relict glacial catchments and formerly glaciated regions are italicized. ^ denotes meltwater plume deposits with no till counterpart presented in Fig. 5. * indicates samples examined for microtexture analysis. Intervals indicate depths in the sediment cores (with core top depth = 0) from which samples within the facies of interest were collected (lithological boundaries were avoided). Negative elevation indicates water depth of a core site, while positive elevation is used for the altitude of a site with relatively unaltered source materials used as references. MPD = meltwater plume deposit; GZ = grounding zone; Diam. = diamicton.

Core ID	Interval cm	Latitude	Longitude	Elevation m	Facies	Glacial Catchment/Region	Reference
Ryder19-6-GC	184-185	80.0095	-51.7408	-633	MPD	Ryder Glacier	O'Regan et al., 2021
Ryder19-7-PC	594-595	81.9518	-51.5878	-559	MPD	Ryder Glacier	O'Regan et al., 2021
Ryder19-7-PC *	878-879	81.9518	-51.5878	-559	Subglacial till	Ryder Glacier	O'Regan et al., 2021
Ryder19-8-PC *	920-921	81.8928	-51.1315	-238	Subglacial till	Ryder Glacier	O'Regan et al., 2021
Ryder19-9-PC *	622-623	81.8908	-50.9682	-274	MPD	Ryder Glacier	O'Regan et al., 2021
Ryder19-9PC *	830-831	81.8908	-50.9682	-274	MPD	Ryder Glacier	O'Regan et al., 2021
OD1507-18-GC ^	160-161	81.6266	-62.2989	-520	MPD	Petermann Glacier	Jennings et al., 2022
OD1507-31-PC ^	560-561	81.6106	-64.3522	-569	MPD	Nares Ice Stream	Jennings et al., 2022
CAGE-15-5-1221-GC	17-18	73.6098	34.6908	-253	MPD	*Thor Iversenbanken*	Esteves et al., 2022
CAGE-15-5-1221-GC	32-33	73.6098	34.6908	-253	MPD	*Thor Iversenbanken*	Esteves et al., 2022
CAGE-15-5-1221-GC	48-49	73.6098	34.6908	-253	Subglacial till	*Thor Iversenbanken*	Esteves et al., 2022
CAGE-15-5-1221-GC	61-62	73.6098	34.6908	-253	Subglacial till	*Thor Iversenbanken*	Esteves et al., 2022
CAGE-15-5-1222-GC	103-104	73.6173	34.6011	-310	MPD	*Thor Iversenbanken*	Esteves et al., 2022
CAGE-15-5-1222-GC	117-118	73.6173	34.6011	-310	MPD	*Thor Iversenbanken*	Esteves et al., 2022
CAGE-15-5-1222-GC	126-127	73.6173	34.6011	-310	Subglacial till	*Thor Iversenbanken*	Esteves et al., 2022
CAGE-15-5-1222-GC	133-134	73.6173	34.6011	-310	Subglacial till	*Thor Iversenbanken*	Esteves et al., 2022
JM-KA09-GC ^	341-342	74.8819	17.2035	-274	MPD	*Kveithola Ice Stream*	Rüther et al., 2012
DF85-115-PC	145-146	-68.4433	-70.7633	-726	MPD	*Marguerite Trough Ice Stream*	Kennedy & Anderson, 1989
DF85-115-PC	180-181	-68.4433	-70.7633	-726	MPD	*Marguerite Trough Ice Stream*	Kennedy & Anderson, 1989
DF85-115-PC	200-201	-68.4433	-70.7633	-726	Subglacial till	*Marguerite Trough Ice Stream*	Kennedy & Anderson, 1989
DF85-115-PC	205-206	-68.4433	-70.7633	-726	Subglacial till	*Marguerite Trough Ice Stream*	Kennedy & Anderson, 1989
DF85-116-PC	26-27	-68.4833	-70.6000	-650	MPD	*Marguerite Trough Ice Stream*	Kennedy & Anderson, 1989

Core ID	Interval *cm*	Latitude	Longitude	Elevation *m*	Facies	Glacial Catchment/Region	Reference
DF85-116-PC	82-83	-68.4833	-70.6000	-650	MPD	*Marguerite Trough Ice Stream*	Kennedy & Anderson, 1989
DF85-116-PC	102-103	-68.4833	-70.6000	-650	Subglacial till	*Marguerite Trough Ice Stream*	Kennedy & Anderson, 1989
DF85-116-PC	143-144	-68.4833	-70.6000	-650	Subglacial till	*Marguerite Trough Ice Stream*	Kennedy & Anderson, 1989
OSO09-10 KC04*	3-4	-72.6971	-107.1105	-729	MPD	Pine Island Glacier	Witus et al., 2014
OSO09-10 KC04	200-201	-72.6971	-107.1105	-729	Subglacial till	Pine Island Glacier	Witus et al., 2014
OSO09-10 KC18	30-31	-73.3835	-106.871	-894	MPD	Pine Island Glacier	Kirshner et al., 2012
OSO09-10 KC25	75-76	-73.2570	-107.1057	-838	Subglacial till	Pine Island Glacier	Kirshner et al., 2012
PIG-B	1-2	-75.0754	-100.432	-725	MPD	Pine Island Glacier	Smith et al., 2017
PIG-B	18-19	-75.0754	-100.432	-725	GZ- proximal diam.	Pine Island Glacier	Smith et al., 2017
PIG-B	80-81	-75.0754	-100.432	-725	GZ- proximal diam.	Pine Island Glacier	Smith et al., 2017
NBP20-02 KC26 *	70-72	-75.0215	-100.7513	-805	GZ- proximal diam.	Pine Island Glacier	This study
NBP19-02 KC04	170-172	-74.94	-106.18	-469	GZ- proximal diam.	Thwaites Glacier	Lepp et al., 2022
NBP19-02 KC13	10-12	-74.911	-106.953	-463	MPD	Thwaites Glacier	Clark et al., 2024
NBP19-02 JGC11	62-63	-75.058	-107.299	-752	GZ- proximal diam.	Thwaites Glacier	Clark et al., 2024
NBP19-02 KC15 *	80-82	-74.871	-106.333	-545	MPD	Thwaites Glacier	Clark et al., 2024
NBP19-02 JGC17	6-7	-74.887	-106.316	-507	MPD	Thwaites Glacier	Clark et al., 2024
NBP19-02 JGC17	106-107	-74.887	-106.316	-507	GZ- proximal diam.	Thwaites Glacier	Clark et al., 2024
NBP19-02 KC23	60-62	-75.07	-104.23	-677	GZ- proximal diam.	Thwaites Glacier	Lepp et al., 2022
NBP19-02 KC23	130-132	-75.07	-104.23	-677	GZ- proximal diam.	Thwaites Glacier	Lepp et al., 2022
NBP20-02 KC33	200-202	-74.64	-106.18	-397	MPD	Thwaites Glacier	Lepp et al., 2022
NBP20-02 KC67	50-52	-74.84	-104.46	-613	MPD	Thwaites Glacier	Lepp et al., 2022
NBP15-02 KC17	170-171	-75.874	179.666	-549	MPD	Western Ross Sea	Prothro et al., 2018
NBP15-02 KC19	115-116	-76.03	177.210	-455	Subglacial till	Western Ross Sea	Halberstadt et al., 2018
NBP15-02 KC19	145-146	-76.03	177.210	-455	Subglacial till	Western Ross Sea	Prothro et al., 2018
NBP15-02 KC22 *	115-116	-75.43	176.196	-354	Subglacial till	Western Ross Sea	Halberstadt et al., 2018
NBP15-02 KC22	120-121	-75.43	176.196	-354	Subglacial till	Western Ross Sea	Halberstadt et al., 2018
NBP15-02 KC24	79-80	-75.671	176.446	-450	MPD	Western Ross Sea	Simkins et al., 2017
Qaanaaq_1A	-	77.493	-69.242	372	Cryoconite	Qaanaaq Glacier	This study

Core ID	Interval *cm*	Latitude	Longitude	Elevation *m*	Facies	Glacial Catchment/Region	Reference
Qaanaaq_2A	-	77.496	-69.229	456	Cryoconite	Qaanaaq Glacier	This study
Qaanaaq_3A	-	77.497	-69.200	556	Cryoconite	Qaanaaq Glacier	This study
SDM94	-	-81.643	-148.773	615	Basal ice debris	Siple Dome	This study
19-KP-H6	-	-75.215	-110.960	84	Fringe debris	Kay Peak, Pope Glacier	This study

Table A2: Results of two-tailed Z test and associated p-values performed on grain shape of meltwater plume deposit and till populations from each catchment. Z scores are absolute values. Shape metrics with significantly different populations (Z > 3.0) are shown in bold (Fig. 4). Difference in means for those statistically significant metrics is presented with 95 % confidence interval calculated from 1,000 bootstrap replicates. Note the small values reflect both the range of the metric itself [0, 1] and support the rejection of the null hypothesis that MPD and till sample populations are the same. Abbreviations of the glacial catchments/regions are the same as in Figure 1.

		Ryder	TI	MTIS	PIG	TG	Ross
Circularity	Z-Score	**11.313**	2.1265	0.6375	**3.7678**	0.5258	**6.4984**
	p-value	$< 2.2e^{-16}$	0.173	0.5238	$1.65e^{-4}$	0.599	$8.12e^{-11}$
	Difference in Means	$5.30e^{-2}\ {}^{+9.92e^{-3}}_{-9.68e^{-3}}$	-	-	$1.60e^{-2}\ {}^{+8.34e^{-3}}_{-8.66e^{-3}}$	-	$3.36e^{-2}\ {}^{+1.06e^{-2}}_{-9.68e^{-3}}$
Eccentricity	Z-Score	0.6247	0.4847	**4.7231**	2.5914	0.0144	0.2989
	p-value	0.532	0.386	$2.32e^{-6}$	$9.56e^{-3}$	0.989	0.765
	Difference in Means	-	-	$3.95e^{-2}\ {}^{+1.64e^{-2}}_{-9.52e^{-2}}$	-	-	
Solidity	Z-Score	**9.1276**	1.832	0.1234	**3.214**	1.056	**5.377**
	p-value	$< 2.2e^{-16}$	0.0570	0.9018	$1.31e^{-3}$	0.291	$7.57e^{-8}$
	Difference in Means	$3.34e^{-2}\ {}^{+7.13e^{-3}}_{-6.67e^{-3}}$	-	-	$1.05e^{-2}\ {}^{+6.52e^{-3}}_{-6.28e^{-3}}$	-	$2.02e^{-2}\ {}^{+6.88e^{-3}}_{-7.22e^{-3}}$

Data and Code availability

Author contribution

Competing interests

Acknowledgements

References

635

Alley, R. B., Blankenship, D. D., Bentley, C. R., and Rooney, S. T.: Deformation of till beneath ice stream B, West Antarctica, Nature, 322, 57–59, doi: 10.1038/322057a0, 1986.

Alley, R.B., Cuffey, K.M., Evenson, E.B., Strasser, J.C., Lawson, D.E., and Larson, G.J.: How glaciers entrain and transport basal sediments: physical constraints, Quaternary Sci. Rev., 16, 1017-1038, doi: 10.1016/S0277-3791(97)00034-6, 1997.

Alley, R.B., Cuffey, K.M., and Zoet, L.K.: Glacial erosion: status and outlook, Ann. Glaciol., 60, 1-13, doi: 10.1017/aog.2019.38, 2019.

Anderson, J.B. and Fretwell, L.O.: Geomorphology of the onset area of a paleo-ice stream, Marguerite Bay, Antarctic Peninsula, Earth Surf. Proc. Land., 33, 503-512, doi: 10.1002/esp.1662, 2008.

Andreassen, K. and Winsborrow, M.: Signature of ice streaming in Bjørnøyrenna, Polar North Atlantic, through the Pleistocene and implications for ice-stream dynamics, Ann. Glaciol., 50, 17-26, doi: 10.3189/172756409789624238, 2009.

Bindschadler, R.: The importance of pressurized subglacial water in separation and sliding at the glacier bed, J. Glaciol., 29, 3-19, doi: 10.3189/S0022143000005104, 1983.

Blackman, D.K., Von Herzen, R.P., and Lawver, L.A.: Heat flow and tectonics in the Western Ross Sea, Antarctica, Vol. 5B9, 179-189, Earth Science Series, Circum-Pacific Council for Energy and Mineral Resources, 1987.

Boulton, G.S., Dobbie, K.E., and Zatsepin, S.: Sediment deformation beneath glaciers and its coupling to the subglacial hydraulic system, Quatern. Int., 86, 3-28, doi: 10.1016/S1040-6182(01)00048-9, 2001.

Bowling, J.S., Livingstone, S.J., Sole, A.J., and Chu, W.: Distribution and dynamics of Greenland subglacial lakes, Nat. Commun., 10, 2810, doi: 10.1038/s41467-019-10821-w, 2019.

Bjarnadóttir, L.R., Winsborrow, M.C.M., and Andreassen, K.: Deglaciation of the central Barents Sea, Quaternary Sci. Rev., 92, 208-226, doi: 10.1016/j.quascirev.2013.09.012, 2014.

Campaña, I., Benito-Calvo, A., Pérez-González, Bermúdez de Castro, J.M., and Carbonell, E.: Assessing automated image analysis of sand grain shape to identify sedimentary facies, Gran Dolina archaeological site (Burgos, Spain), Sed. Geol., 346, 72-83, doi: 10.1016/j.sedgeo.2016.09.010, 2016.

Carter, S.P., Fricker, H.A., Blankenship, D.D., Johnson, J.V., Lipscomb, W.H., Price, S.F., and Young, D.A.: Modeling 5 years of subglacial lake activity in the MacAyeal Ice Stream (Antarctica) catchment through assimilation of ICESat laser altimetry, Ann. Glaciol., 57, 1098-1112, doi: 10.3189/002214311798843421, 2011.

Charpentier, I., Staszyc, A.B., Wellner, J.S., and Alejandro, V.: Quantifying grain shape with MorpheoLV: a case study using Holocene glacial marine sediments, EPJ Web of Conferences. Vol. 140. EDP Sciences, doi:10.1051/epjconf/201714014003, 2017.

Clark, R.W., Wellner, J.S., Hillenbrand, C.-D., Totten, R.L., Smith, J.A., Simkins, L.M., Larter, R.D., Hogan, K.A., Graham, A.G.C., Nitsche, F.O., Lehrmann, A.A., Lepp, A.P., Kirkham, J.D., Fitzgerald, V.T., Garcia-Barrera, G., Ehrmann, W., and Wacker, L.: Synchronous retreat of Thwaites and Pine Island glaciers in response to external forcings in the pre-satellite era, P. Natl. Acad. Sci. USA, 121, e2211711120, doi: 10.1073/pnas.2211711120, 2024.

Cooper, A.K., Davey, F.J., and Behrendt, J.C.: The Antarctic Continental Margin: Geology and Geophysics of the Western Ross Sea, Vol. 5B9, 27-65, Earth Science Series, Circum-Pacific Council for Energy and Mineral Resources, 1987.

Cowan, E.A., Hillenbrand, C.-D., Hassler, L.E., and Ake, M.T.: Coarse-grained terrigenous sediment deposition on continental rise drifts: a record of Plio-Pleistocene glaciation on the Antarctic Peninsula, Palaeogeogr. Palaeocl., 265, 275-291, doi: 10.1016/j.palaeo.2008.03.010, 2008.

Cowan, E.A., Christoffersen, P., and Powell, R.D.: Sedimentological signature of a deformable bed preserved beneath an ice stream in a late Pleistocene glacial sequence, Ross Sea, Antarctica, J. Sediment. Res., 82, 270-282, doi: 10.2110/jsr.2012.25, 2012.

Creyts, T.T. and Clarke, G.K.C.: Hydraulics of subglacial supercooling: theory and simulations for clear water flows, J. Geophys. Res.-Earth, 115, F03021, doi: 10.1029/2009JF001417, 2010.

Crompton, J.W., Flowers, G.E., and Dyck, B.: Characterization of glacial silt and clay using automated mineralogy, Ann. Glaciol., 60, 49-65, doi: 10.1017/aog.2019.45, 2019.

27

685 Damiani, T.M., Jordan, T.A., Ferraccioli, F., Young, D.A., and Blankenship, D.D.: Variable crustal thickness beneath Thwaites Glacier revealed from airborne gravimetry, possible implications for geothermal heat flux in West Antarctica, Earth Planet. Sc. Lett., 407, 109-122, doi: 10.1016/j.espl.2014.09.023, 2014.

Domack, E.W., Jacobson, E.K., Shipp, S., and Anderson, J.B.: Late Pleistocene-Holocene retreat of the west Antarctic ice sheet system in the Ross Sea: Part 2 – sedimentologic and stratigraphic signature, Geol. Soc. Am. Bull., 111, 1517-1536, 1999.

690 Dreimanis, A., and Vagners, U.J: Bimodal distribution of rock and mineral fragments in basal tills, Glacial Till: An Interdisciplinary Study, edited by: Legget, R.F., Royal Society of Canada, Special Publication, 12, 237-250, 1971.

Dreimanis, A., and Vagners, U.J.: The effect of lithology upon texture of till, Research methods in Pleistocene geomorphology, 66-82, 1972.

Dziadek, R., Ferraccioli, F., and Gohl, K.: High geothermal heat flow beneath Thwaites Glacier in West Antarctica inferred from aeromagnetic data, Nat. Commun. Earth Environ., 162, doi: 10.1038/s43247-012-00242-3, 2021.

695 Ehrmann, W., Hillenbrand, C.-D., Smith, J.A., Graham, A.G.C., Kuhn, G., and Larter, R.D.: Provenance changes between recent and glacial-time sediments in the Amundsen Sea embayment, West Antarctica: clay mineral assemblage evidence, Antarct. Sci., 23, 471-486, doi: 10.1017/S0954102011000320, 2011.

Esteves, M., Bjarnadóttir, L.R., Winsborrow, M.C.M., Shackleton, C.S., and Andreassen, K.: Retreat patterns and dynamics of the Sentralbankrenna glacial system, central Barents Sea, Quaternary Sci. Rev., 169, 131-147, doi: 10.1016/j.quascirev.2017.06.004, 2017.

700 Esteves, M., Rüther, D., Winsborrow, M. C. M., Livingstone, S. J., Shackleton, C. S., and Andreassen, K.: An interconnected palaeo-subglacial lake system in the central Barents Sea, EarthArxiv [ArXiv pre-print], doi:10.31223/X58934, 2022.

Evans D.J.A., Phillips, E.R., Hiemstra, J.F., and Auton, C.A.: Subglacial till: Formation, sedimentary characteristics and classification, Earth-Sci. Rev, 78, 115-176, doi: 10.1016/j.earscirev.2006.04.001, 2006.

705 Evans, J., Pudsey, C.J., Ó Cofaigh, C., Morris, P., and Domack, E.: Late Quaternary glacial history, flow dynamics, and sedimentation along the eastern margin of the Antarctic Peninsula Ice Sheet, Quaternary Sci. Rev., 24, 741-774, doi: 10.1016/j.quascirev.2004.10.007, 2005.

Flowers, G.E.: Hydrology and the future of the Greenland Ice Sheet, Nat. Commun., 9, 2729, doi: 10.1038/s41467-018-05002-0, 2018.

710 Fricker, H.A., Scambos, T., Bindschadler, R., and Padman, L.: An active subglacial water system in West Antarctica mapped from space, Science, 315, 1544-1548, doi: 10.1126/science.1136897, 2007.

Gilbert, E., and Kittel, C.: Surface melt and runoff on Antarctic ice shelves at 1.5 °C, 2 °C, and 4 °C of future warming, Geophys. Res. Lett., 48, e2020GL091733, doi: 10.1029/2020GL091733, 2021.

715 Greco, N., and Jaeger, J.M.: Modeling Mud: Flocs as Global Meltwater Indicators in Ice-Proximal Glacimarine Sediments, *AGU Fall Meeting Abstracts*, 2020, EP001-0014, 2020.

Greenwood, S. L., Gyllencreutz, R., Jakobsson, M., and Anderson, J. B.: Ice-flow switching and East/West Antarctic Ice Sheet roles in glaciation of the western Ross Sea, Geol. Soc. Am. Bull., 124, 1736–1749, doi:10.1130/B30643.1, 2012.

720 Greenwood, S.L., Clason, C.C., Helanow, C., and Margold, M.: Theoretical, contemporary observational and palaeo-perspectives on ice sheet hydrology: Processes and products, Earth Sci. Rev., 15, 1-27, doi:10.1016/j.earscirev.2016.01.010, 2016.

Greenwood, S. L., Simkins, L. M., Winsborrow, M. C. and Bjarnadóttir, L. R. Exceptions to bed-controlled ice sheet flow and retreat from glaciated continental margins worldwide. Sci. Adv. 7, doi:10.1126/sciadv.abb6291, 2021.

725 Gustafson, C.D., Key, K., Siegfried, M.R., Winberry, J.P., Fricker, H.A., Venturelli, R.A., and Michaud, A.B.: A dynamic saline groundwater system mapped beneath an Antarctic ice stream, Science, 376, 640-644, doi: 10.1126/science.abm3301, 2022.

Halberstadt, A.R.W, Simkins, L., Greenwood, S., and Anderson, J., Past ice-sheet behaviour: Retreat scenarios and changing controls in the Ross Sea, Antarctica, Cryosphere, 10, 1003-1020, doi: 10.5194/tc-10-1003-2016, 2016.

730 Halberstadt, A.R.W., Simkins, L.M., Anderson, J.B., Prothro, L.O., and Bart, P.J.: Characteristics of the deforming bed: till properties on the deglaciated Antarctic continental shelf. J. Glaciol., 64, 1014-1027, doi: 10.1017/jog.2018.92, 2018.

28

Haldorsen, S.: Grain-size distribution of subglacial till and its relation to glacial crushing and abrasion, Boreas, 10, 91-105, doi: 10.1111/j.1502-3885.1981.tb00472.x, 1981.

735   Hart, J.K.: Athabasca Glacier, Canada – a field example of subglacial ice and till erosion? Earth Surf. Proc. Land., 31, 65-80, doi: 10.1002/esp.1233, 2006.

Hillenbrand, C.-D., Grobe, H., Diekmann, B., Kuhn, G., and Fütterer, D.K.: Distribution of clay minerals and proxies for productivity in surface sediments of the Bellingshausen and Amundsen seas (West Antarctica) – relation to modern environmental conditions, Mar. Geol., 193, 253-271, doi: 10.1016/S0025-3227(02)00659-X, 2003.

740   Hillenbrand, C.-D., Kuhn, G., Smith, J.A., Gohl, K., Graham, A.G.C., Larter, R.D., Klages, J.P., Downey, R., Moreton, S.G., Forwick,M., and Vaughan, D.G.: Grounding-line retreat of the West Antarctic Ice Sheet from inner Pine Island Bay, Geology, 41, 35-38, doi: 10.1130/G33469.1, 2013.

Hoffman, A.O., Christianson, K., Shapero, D., Smith, B.E., and Joughin, I.: Brief Communication: Heterogenous thinning and subglacial lake activity on Thwaites Glacier, West Antarctica, Cryosphere, 14, 4603-4609, doi: 10.5194/tc-14-4603-2020, 2020.

745   Hogan, K.A., Jakobsson, M., Mayer, L., Reilly, B.T., Jennings, A.E., Stoner, J.S., Nielsen, T., Andresen, K.J., Nørmark, E., Heirman, K.A., Kamla, E., Jerram, K., Stranne, C., and Mix, A.: Glacial sedimentation, fluxes, and erosion rates associated with ice retreat in Petermann Fjord and Nares Strait, north-west Greenland, Cryosphere, 14, 261-286, doi: 10.5194/tc-14-261-2020, 2020a.

750   Hogan, K.A., Larter, R.D., Graham, A.G.C., Arthern, R., Kirkham, J.D., Minzoni, R.T., Jordan, T.A., Clark, R., Fitzgerald, V., Wåhlin, A.W., Anderson, J.B., Hillenbrand, C.-D., Nitsche, F.O., Simkins, L., Smith, J.A., Gohl, K., Arndt, J.E., Hong, J., and Wellner, J.: Revealing the former bed of Thwaites Glacier using sea-floor bathymetry: implications for warm-water routing and bed controls on ice flow and buttressing, Cryosphere, 14, 2883–2908, doi: 10.5194/tc-14-2883-2020, 2020b.

755   Hogan, K.A., Arnold, N.S., Larter, R.D., Kirkham, J.D., Noormets, R., Ó Cofaigh, C., Golledge, N.R., and Dowdeswell, J.A.: Subglacial water flow over an Antarctic palaeo-ice stream bed, , J. Geophys. Res.-Earth, 127, e2021JF006442, doi: 10.1029/2021JF006442, 2022.

Immonen, N.: Surface microtextures of ice-rafted quartz grains revealing glacial ice in the Cenozoic Arctic, Palaeogeogr. Palaeocl., 374, 293-302, doi: 10.1016/j.palaeo.2013.02.003, 2013.

760   Iverson, N.R., Hooyer, T.S., and Hooke, R.L.: A laboratory study of sediment deformation: stress heterogeneity and grain-size evolution, Ann. Glaciol., 22, 167-175, doi: 10.3189/1996AoG22-1-167-175, 1996.

Iverson, N.R.: Shear resistance and continuity of subglacial till: hydrology rules, J. Glaciol., 56, 1104-1114, doi: 10.3189/002214311796406220, 2010.

Iverson, N.R., McCracken, R.G., Zoet, L.K., Benediktsson, Í. Ö., Schomacker, A., Johnson, M.D., and Woodard, J.: A
765   theoretical model of drumlin formation based on observations at Múlajökull, Iceland, J. Geophys. Res.-Earth, 122, 2302-2323, doi: 10.1002/2017JF004354, 2017.

Jakobsson, M., Hogan, K.A., Mayer, L.A., Mix, A., Jennings, A., Stoner, J., Eriksson, B., Jerram, K., Mohammad, R., Pearce, C., Reilly, B., and Stranne, C.: The Holocene retreat dynamics and stability of Petermann Glacier in northwest Greenland, Nat. Commun., 9, 2104, doi: 10.1038/s41467-018-04573-2, 2018.

770   Jennings, A., Reilly, B., Andrews, J., Hogan, K., Walczak, M., Jakobsson, M., Stoner, J., Mix, A., Nicholls, K.W., O'Regan, M., Prins, M.A., and Troelstra, S.R.: Modern and early Holocene ice shelf sediment facies from Petermann Fjord and northern Nares Strait, northwest Greenland, Quaternary Sci. Rev., 283, 107460, doi: 10.1016/j.quascirev.2022.107460, 2022.

Kennedy, D.S. and Anderson, J.B.: Glacial-marine sedimentation and Quaternary glacial history of Marguerite Bay,
775   Antarctic Peninsula, Quaternary Res., 31, 255-276, doi: 10.1016/0033-5894(89)90008-2, 1989.

Kilfeather, A.A., Ó Cofaigh, C., Lloyd, J.M., Dowdeswell, J.A., Xu, S., and Moreton, S.G.: Ice-stream retreat and ice-shelf history in Marguerite Trough, Antarctic Peninsula: Sedimentological and foraminiferal signatures, Geol. Soc. Am. Bull., 123, 997-1015, doi: 10.1130/B30282.1, 2011.

Kirkham, J.D., Hogan, K.A., Larter, R.D., Arnold, N.S., Nitsche, F.O., Goleldge, N.R., and Dowdeswell, J.A.: Past water
780   flow beneath Pine Island and Thwaites glaciers, West Antarctica, Cryosphere, 13, 1959-1981, doi:10.5194/tc-13-1959-2019, 2019.

Kirkham, J.D., Hogan, K.A., Larter, R.D., Arnold, N.S., Nitsche, F.O., Kuhn, G., Gohl, K., Anderson, J.B., and Dowdeswell, J.A.: Morphometry of bedrock meltwater channels on Antarctic inner continental shelves: Implications for channel development and subglacial hydrology, Geomorphology, 370, 107369, doi: 10.1016/j.geomorph.2020.107369, 2020.

Kirshner, A.E., Anderson, J.B., Jakobsson, M., O'Regan, M., Majewski, W., and Nitsche, F.O.: Post-LGM deglaciation in Pine Island Bay, West Antarctica, Quaternary Sci. Rev., 38, 11-26, doi: 10.1016/j.quascirev.2012.01.017, 2012.

Křížek, M., Krbcová, K., Mida, P., and Hanáček, M.: Micromorphological changes as an indicator of the transition from glacial to glaciofluvial quartz grains: Evidence from Svalbard, Sediment. Geol., 358, 35-43, doi:10.1016/j.sedgeo.2017.06.010, 2017.

Kuhn, G., Hillenbrand, C.-D., Kasten, S., Smith, J.A., Nitsche, F.O., Frederichs, T., Wiers, S., Ehrmann, W., Klages, J.P., and Mogollon, J.M.: Evidence for a palaeo-subglacial lake on the Antarctic continental shelf, Nat. Commun., 8, 15591, doi: 10.1038/ncomms15591, 2017.

Kurtz, D.D. and Anderson, J.B.: Recognition and sedimentologic description of recent debris flow deposits from the Ross and Weddell seas, Antarctica, J. Sediment. Res., 49, 1159-1169, doi: 10.1306/212F78D8-2B24-11D7-86480000102C1865D, 1979.

Larter, R.D., Anderson, J.B., Graham, A.G.C., Gohl, K., Hillenbrand, C.-D., Jakobsson, M., Johnson, J.S., Kuhn, G., Nitsche, F.O., Smith, J.A., Witus, A.E., Bentley, M.J., Dowdeswell, J.A., Ehrmann, W., Klages, J.P., Lindow, J., Ó Cofaigh, C., and Spiegel, C.: Reconstruction of changes in the Amundsen Sea and Bellingshausen Sea sector of the West Antarctic Ice Sheet since the Last Glacial Maximum, Quaternary Sci. Rev., 100, 55-86, doi: 10.1016/j.quascirev.2013.10.016, 2014.

Lecavalier, B.S., Fisher, D.A., Milne, G.A., Vinther, B.M., Tarasov, L., Huybrechts, P., Lacelle, D., Main, B., Zheng, J., Bourgeois, J., and Dyke, A.S.: High Arctic Holocene temperature record from the Agassiz ice cap and Greenland ice sheet evolution, P. Natl. Acad. Sci. USA, 114, 5952-5957, doi: 10.1073/pnas.1616287114, 2017.

Leidman, S.Z., Rennermalm, A.K., Muthyala, R., Guo, Q., and Overeem, I.: The presence and widespread distribution of dark sediment in Greenland Ice Sheet supraglacial streams implies substantial impact of microbial communities on sediment deposition and albedo, Geophys. Res. Lett., 48, 2020GL088444, doi: 10.1029/2020GL088444, 2020.

Lenaerts, J.T.M., Vizcaino, M., Fyke, J., van Kampenhout, L., and van den Broeke, M.R.: Present-day and future Antarctic ice sheet climate and surface mass balance in the Community Earth System Model, Clim. Dynam., 47, 1367-1381, doi: 10.1007/s00382-015-2907-4, 2016.

Lepp, A.P., Simkins, L.M., Anderson, J.B., Clark, R.W., Wellner, J.S., Hillenbrand, C.-D., Smith, J.A., Lehrmann, A.A., Totten, R., Larter, R.D., Hogan, K.A., Nitsche, F.O., Graham, A.G.C., and Wacker, L.: Sedimentary signatures of persistent subglacial meltwater drainage from Thwaites Glacier, Antarctica, Front. Earth Sci., 10:863200, doi: 10.3389/feart.2022.863200, 2022.

Lepp, A.P., Miller, L.E., Anderson, J.B., O'Regan, M., Winsborrow, M., Smith, J., Hillenbrand, C.-D., Wellner, J., Prothro, L., and Podolskiy, E.: Grain shape and microtexture of glacial silt-sized sediments from Antarctica, Northwest Greenland, and the central Barents Sea, PANGAEA [data set], doi: 10.1594/PANGAEA.961704, 2023.

Lešić, N.-M., Streuff, K.T., Bohrmann, G., and Kuhn, G.: Glacimarine sediments from outer Drygalski Trough, sub-Antarctic South Georgia – evidence for extensive glaciation during the Last Glacial Maximum, Quaternary Sci. Rev., 292, 107657, doi: 10.1016/j.quascirev.2022.107657, 2022.

Licht, K.J., Dunbar, N.W., Andrews, J.T., and Jennings, A.E.: Distinguishing subglacial till and glacial marine diamictons in the western Ross Sea, Antarctica: Implications for a last glacial maximum grounding line, GSA Bulletin, 111, 91-103, doi: 10.1130/0016-7606(1999)111<0091:DSTAGM>2.3.CO;2, 1999.

Licht, K.J., Lederer, J.R., and Swope, R.J.: Provenance of LGM glacial till (sand fraction) across the Ross embayment, Antarctica, Quaternary Sci. Rev., 24, 1499-1520, doi: 10.1016/j.quascirev.2004.10.017, 2005.

Livingstone, S.J., Ó Cofaigh, C., Stokes, C.R., Hillenbrand, C.-D., Vieli, A., and Jamieson, S.S.R.: Glacial geomorphology of Marguerite Bay Palaeo-Ice stream, western Antarctic Peninsula, J. Maps, 9, 558-572, doi: 10.1080/17445647.2013.829411, 2013.

Livingstone, S.J., Li, Y., Rutishauser, A., Sanderson, R.J., Winter, K., Mikucki, J.A., Björnsson, H., Bowling, J.S., Chu, W., Dow, C.F., Fricker, H.A., McMillan, M., Ng, F.S.L., Ross, N., Sieger, M.J., Siegfried, M., and Sole, A.J.:

Subglacial lakes and their changing role in a warming climate, Nat. Rev. Earth Environ., 3, 106-124, doi: 10.1038/s43017-021-00246-9, 2022.

Livsey, D.N., Simms, A.R., Clary, W.G., Wellner, J.S., Anderson, J.B., and Chandler, J.P.: Fourier grain-shape analysis of Antarctic marine core: the relative influence of provenance and glacial activity on grain shape, J. Sediment. Res., 83, 80-90, doi: 10.2110/jrs.2013.5, 2013.

Mahaney, W.C.: Atlas of sand grain surface textures and applications, Oxford University Press, USA, 2002.

Malczyk, G., Gourmelen, N., Goldberg, D., Wuite, J., and Nagler, T.: Repeat subglacial lake drainage and filling beneath Thwaites Glacier, Geophys. Res. Lett., 47, e2020GL089658, doi: 10.1029/2020GL089658, 2020.

Manning, A.J., Spearman, J.R., Whitehouse, R.J.S., Pidduck, E.L., Baugh, J.V., and Spencer, K.L.: Flocculation Dynamics of Mud: San Mixed Suspensions, in: Sediment transport processes and their modelling applications, edited by: Manning, A.J., InTech, Rijeka, Croatia, 119-125, doi:10.5772/55233, 2013.

Marsaglia, K., Milliken, K., and Doran, L.: IODP digital reference for smear slide analysis of marine mud. Part 1: Methodology and atlas of siliciclastic and volcanogenic components, IODP Technical Note 1, doi: 10.2204/iodp.tn.1.2013, 2013.

McCave, I.N., Manighetti, B., and Robinson, S.G.: Sortable silt and fine sediment size/composition slicing: Parameters for palaeocurrent speed and palaeoceanography, Paleoceanography and Paleoclimatology, 10, 593-610, doi: 10.1029/94PA03039, 1995.

McFarlin, J.M., Axford, Y., Osburn M.R., Kelly, M.A., Osterberg, E.C., and Farnsworth, L.B.: Pronounced summer warming in northwest Greenland during the Holocene and Last Interglacial, P. Natl. Acad. Sci. USA, 201720420, doi: 10.1073/pnas.1720420115, 2018.

Menzies, J.: Strain pathways, till internal architecture and microstructures-perspectives on a general kinematic model – a 'blueprint' for till development, Quaternary Sci. Rev., 50, 105-124, doi: 10.1016/j.quascirev.2012.07.012, 2012.

Meyer, C.R., Robel, A.A., and Rempel, A.W.: Frozen fringe explains sediment freeze-on during Heinrich events, Earth Plan. Sci. Lett., 524, 115725, doi: 10.1016/j.eosl.2019/115725, 2019.

Munoz, Y.P. and Wellner, J.S.: Seafloor geomorphology of western Antarctic Peninsula bays: a signature of ice flow behavior, Cryosphere, 12, 205-225, doi: 10.5194/tc-12-205-2018, 2018.

Muto, A., Peters, L.E., Gohl, K., Sasgen, I., Alley, R.B., Anandakrishnan, S., and Riverman, K.L.: Subglacial bathymetry and sediment distribution beneath Pine Island Glacier ice shelf modeled using aerogravity and in situ geophysical data: new results, Earth Planet. Sc. Lett., 443, 63-75, doi: 10.1016/j.epsl.2015.10.037, 2016.

Nitsche, F.O., Gohl, K., Larter, R.D., Hillenbrand, C.D., Kuhn, G., Smith, J.A., Jacobs, S., Anderson, J.B., and Jakobsson, M.: Paleo ice flow and subglacial meltwater dynamics in Pine Island Bay, West Antarctica, Cryosphere, 7, 249–262, doi:10.5194/tc-7-249-2013, 2013.

Ó Cofaigh, C. and Dowdeswell, J.A.: Laminated sediments in glacimarine environments: diagnostic criteria for their interpretation, Quaternary Sci. Rev., 20, 1411-1436, doi: 10.1016/S0277-3791(00)00177-3, 2001.

Ó Cofaigh, C., Dowdeswell, J.A., Allen, C.S., Hiemstra, J.F., Pudsey, C.J., Evans, J., and Evans, D.J.A.: Flow dynamics and till genesis associated with a marine-based Antarctic palaeo-ice stream, Quaternary Sci. Rev., 24, 709-740, doi: 10.1016/j.quascirev.2004.10.006, 2005.

Ó Cofaigh, C., Davies, B.J., Livingstone, S.J., Smith, J.A., Johnson, J.S., Hocking, E.P., Hodgson, D.A., Anderson, J.B., Bentley, M.J., Canals, M., Domack, E., Dowdeswell, J.A., Evans, J., Glasser, N.F., Hillenbrand, C.-D., Larter, R.D., Roberts, S.J., and Simms, A.R.: Reconstruction of ice-sheet changes in the Antarctic Peninsula since the Last Glacial Maximum, Quaternary Sci. Rev., 100, 87-100, doi: 10.1016/j.quascirev.2014.06.023, 2014.

Oakey, R.J., Green, M., Carling, P.A., Lee, M.W.E., Sear, D.A., and Warburton, J.: Grain-shape analysis – a new method for determining representative particle shapes for populations of natural grains, J. Sediment. Res., 75, 1065-1073, doi: 10.2110/jsr.2005.079, 2005.

O'Regan, M., Cronin, T.M., Reilly, B., Alstrup, A.K.O., Gemery, L., Golub, A., Mayer, L.A., Morlighem, M., Moros, M., Munk, O.L., Nilsson, J., Pearce, C., Detlef, H., Stranne, C., Vermassen, F., West, G., and Jakobsson, M.: The Holocene dynamics of Ryder Glacier and ice tongue in north Greenland, Cryosphere, 15, 4073–4097, doi:10.5194/tc-15-4073-2021, 2021.

Passchier, S., Hansen, M.A., and Rosenberg, J.: Quartz grain microtextures illuminate Pliocene periglacial sand fluxes on the Antarctic continental margin, the Depositional Record, 7, 564-581, doi: 10.1002/dep2.157, 2021.

Prothro, L.O., Simkins, L.M., Majewski, W., and Anderson, J.B.: Glacial retreat patterns and processes determined from integrated sedimentology and geomorphology records. Mar. Geol., 395, 104-119, doi:10.1016/j.margeo.2017.09.012, 2018.

885 Reinardy, B.T.I., Hiemstra, J.F., Murray, T., Hillenbrand, C.-D., and Larter, R.D.: Till genesis at the bed of an Antarctic Peninsula palaeo-ice stream as indicated by micromorphological analysis, Boreas, 40, 498-517, doi: 10.1111/j.1502-3885.2010.00199.x, 2011.

Rempel, A.W.: A theory for ice-till interactions and sediment entrainment beneath glaciers, J. Geophys. Res.-Earth, 113, F01013, doi: 10.1029/2007/JF000870, 2008.

Rilling, S., Mukasa, S., Wilson, T., Lawver, L., and Hall, C.: New determinations of 40Ar/39
890 Ar isotopic ages and flow volumes for Cenozoic volcanism in the Terror Rift, Ross Sea, Antarctica, J. Geophys. Res. 114, B12207, doi:10.1029/2009JB006303, 2009.

Robinson, D.E., Menzies, J., Wellner, J.S., and Clark, R.W.: Subglacial sediment deformation in the Ross Sea, Antarctica, Quaternary Sci. Adv., 4, 100029, doi:10.1016/j.qsa.2021.100029, 2021.

Rose, K.C., and Hart, J.K.: Subglacial comminution in the deforming bed: inferences from SEM analysis, Sediment. Geol.,
895 203, 87-97, doi: 10.1016/j.sedgeo.2007.11.003, 2008.

Roseby, Z.A., Smith, J.A., Hillenbrand, C.-D., Cartigny, M.J.B., Rosenheim, B.E., Hogan, K.A., Allen, C.S., Leventer, A., Kuhn, G., Ehrmann, W., and Larter, R.D.: History of Anvers-Hugo Trough, western Antarctic Peninsula shelf, since the Last Glacial Maximum. Part I: Deglacial history based on new sedimentological and chronological data, Quaternary Sci. Rev., 291, 107590, doi: 10.1016/j.quascirev.2022.107590, 2022.

900 Rüther, D.C., Bjarnadóttir, L.R., Junttila, J., Husum, K., Rasmussen, T.L., Lucchi, R.G., and Andreassen, K.: Pattern and timing of the northwestern Barents Sea Ice Sheet deglaciation and indications of episodic Holocene deposition, Boreas, 41, 494-512, doi: 10.1111/j.1502-3885.2011.00244.x, 2012.

Schroeder, D.M., Blankenship, D.D., and Young, D.A.: Evidence for a water system transition beneath Thwaites Glacier, West Antarctica, P. Natl. Acad. Sci. USA, 110, 12225-12228, doi:10.1073/pnas.1302828110, 2013.

905 Schroeder, D.M., Blankenship, D.D., Young, D.A., Witus, A.E., and Anderson, J.B.: Airborne radar sounding evidence for deformable sediments and outcropping bedrock beneath Thwaites Glacier, West Antarctica, Geophys. Res. Lett, 41, 7200, 7208, doi: 10.1002/2014GL061645, 2014.

Schroeder, D.M., MacKie, E.J., Creyts, T.T., and Anderson, J.B.: A subglacial hydrologic drainage hypothesis for silt sorting and deposition during retreat in Pine Island Bay, Ann. Glaciol., 60, 14–20, doi:10.1017/aog.2019.44, 2019.

910 Siegfried, M.R., Fricker, H.A., Carter, S.P., and Tulaczyk, S.: Episodic ice velocity fluctuations triggered by a subglacial flood in West Antarctica, Geophys. Res. Lett., 43, 2640-2648, doi: 10.1002/2016GL067758, 2016.

Siegfried, M.R., Venturelli, R.A., Patterson, M.O., Arnuk, W., Campbell, T.D., Gustafson, C.D., Michaud, A.B., Galton-Fenzi, B.K., Hausner, M.B., Holzschuh, S.N., Huber, B., Manoff, K.D., Schroeder, D.M., Summers, P.T., Tyler, S., Carter, S.P., Fricker, H.A., Harwood, D.M., Leventer, A., Rosenheim, B.E., Skidmore, M.L., Priscu, J.C., and the
915 SALSA Science Team: The life and death of a subglacial lake in West Antarctica, Geology, 51, 434-438, doi: 10.1130/G50995.1, 2023.

Simkins, L.M., Anderson, J.B., Prothro, L.O., Halberstadt, A.R.W., Stearns, L.A., Pollard, D., and DeConto, R.M.: Anatomy of a meltwater drainage system beneath the ancestral East Antarctic ice sheet, Nat. Geosci., 10, 691-697, doi:10.1038/ngeo3012, 2017.

920 Simkins, L.M., Greenwood, S.L., and Anderson, J.B.: Diagnosing ice sheet grounding line stability from landform morphology, Cryosphere, 12, 2707-2726, doi:10.5194/tc-12-2707-2018, 2018.

Simkins, L.M., Greenwood, S.L., Winsborrow, M.C.M., Bjarnadóttir, L.R., and Lepp, A.P.: Advances in understanding subglacial meltwater drainage from past ice sheets, Ann. Glaciol., 1-5, doi: 10.1017/aog.2023.16, 2023.

Simões Pereira, P., van de Flierdt, T., Hemming, S.R., Frederichs, T., Hammond, S.J., Brachfeld, S., Doherty, C., Kuhn, G.,
925 Smith, J.A., Klages, J.P., and Hillenbrand, C.-D.: The geochemical and mineralogical fingerprint of West Antarctica's weak underbelly: Pine Island and Thwaites glaciers, Chem. Geol., 550, 119649, doi: 10.1016/j.chemgeo.2020.119649, 2020.

Smith, A.M., Jordan, T.A., Ferraccioli, F., and Bingham, R.G.: Influence of subglacial conditions on ice stream dynamics: seismic and potential field data from Pine Island Glacier, West Antarctica, J. Geophys. Res.-Earth, 118, 1471-1482,
930 doi: 10.1029/2012JB009582, 2013.

Smith, J.A., Anderson, T.J., Shortt, M., Gaffney, A.M., Truffer, M., Stanton, T.P., Bindschadler, R., Dutrieux, P., Jenkins, A., Hillenbrand, C.-D., Ehrmann, W., Corr, H.F.J., Farley, N., Crowhurst, S., and Vaughan, D.G.: Sub-ice-shelf sediments record history of twentieth-century retreat of Pine Island Glacier, Nature, 541, 77-80, doi: 10.1038/nature20136, 2017.

935   Smith, J.A., Graham, A.G.C., Post, A.L., Hillenbrand, C.-D., Bart, P.J., and Powell, R.D.: The marine geological imprint of Antarctic ice shelves, Nat. Commun., 10, 5635, doi: 10.1038/s41467-019-13496-5, 2019.

St. John, K., Passchier, S., Tantillo, B., Darby, D., and Kearns, L.: Microtextures of modern sea-ice-rafted sediment and implications for paleo-sea-ice reconstructions, Ann. Glaciol., 56, 83-93, doi: 10.3189/2015AoG69A586, 2015.

Stearns, L. A., Smith, B. E., and Hamilton, G. S.:Increased flow speed on a large East Antarctic outlet glacier caused by

940   subglacial floods, Nat. Geosci. Letters, 1, 827-831, doi:10.1038/ngeo356, 2008.

Streuff, K., Ó Cofaigh, C., Hogan, K., Jennings, A., Lloyd, J.M., Noormets, R., Nielsen, T., Juijpers, A., Dowdeswell, J.A., and Weinrebe, W.: Seafloor geomorphology and glacimarine sedimentation associated with fast-flowing ice sheet outlet glaciers in Disko Bay, West Greenland, Quaternary Sci. Rev., 169, 206-230 doi: 10.1016/j.quascirev.2017.05.021, 2017.

945   Sweet, D.E., and Brannan, D.K.: Proportion of glacially to fluvially induced quartz grain microtextures along the Chitina River, SE Alaska, U.S.A., J. Sediment. Res., 86, 749-761, doi: 10.2110/jsr.2016.49, 2016.

Trusel, L.D., Frey, K.E., Das, S.B., Karnauskas, K.B., Munneke, P.K., van Meijgaard, E., and van den Broeke, M.R.: Divergent trajectories of Antarctic surface melt under two twenty-first-century climate scenarios, Nat. Geosci., 8, 927-932, doi: 10.1038/ngeo2563, 2015.

950   van Hateren, J.A., van Buuren, U., Arens, S.M., van Balen, R.T., and Prins, M.A.: Identifying sediment transport mechanisms from grain size-shape distributions, applied to aeolian sediments, Earth Surf. Dynam., 8, 527-553, doi:10.5194/esurf-8-527-2020, 2020.

Vlieghe, M., Coufort-Saudejaud, C., Frances, C., and Liné, A.: In situ characterization of floc morphology by image analysis in a turbulent Taylor-Couette reactor, AlChE Journal: Particle Technology and Fluidization, 60, 2389-2403, doi:

955   10.1002/aic.14431, 2014.

Vos, K.,Vandenberghe, N., and Elsen, J.: Surface textural analysis of quartz grains by scanning electron microscopy (SEM): From sample preparation to environmental interpretation, Earth-Sci. Rev., 128, 193-104, doi:10.1016/j.earscirev.2013.10.013, 2014.

Yawar, Z. and Schieber, J.: On the origin of silt laminae in laminated shales, Sediment. Geol., 360, 22-34,

960   doi:10.1016/j.sedgeo.2017.09.001, 2017.

Wellner, J.S., Anderson, J.B., Ehrmann, W., Weaver, F.M., Kirshner, A., Livsey, D., and Simms, A.R.: History of an Evolving Ice Sheet as Recorded in SHALDRIL Cores From the Northwestern Weddell Sea, Antarctica, in: Tectonic, Climatic, and Cryospheric Evolution of the Antarctic Peninsula, American Geophysical Union, Washington, DC, USA, 131-151, doi: 10.1029/2010SP001047, 2011.

965   Wingham, D.J., Siegert, M.J., Shepherd, A., and Muir, A.S.: Rapid discharge connects Antarctic subglacial lakes, Nature, 440, 1033-1036, doi: 10.1038/nature04660, 2006.

Winsborrow, M.C.M., Andreassen, K., Corner, G.D., and Laberg, J.S.: Deglaciation of a marine-based ice sheet: Late Weichselian palaeo-ice dynamics and retreat in the southern Barents Sea reconstructed from onshore and offshore glacial geomorphology, Quaternary Sci. Rev., 29, 424-442, doi: 10.1016/j.quascirev.2009.10.001, 2010.

970   Witus, A.E., Branecky, C.M., Anderson, J.B., Szczucinski, W., Schroeder, D.M., Blankenship, D.D., and Jakobsson, M.: Meltwater intensive retreat in polar environments and investigation of associated sediments: example from Pine Island Bay, West Antarctica, Quaternary Sci. Rev., 85, 99–118, doi:10.1016/j.quascirev.2013.11.021, 2014.